EXPERIMENTAL DESIGN FOR THE EVALUATION OF HIGH-Tc SUPERCONDUCTIVE THERMAL BRIDGES IN A SENSOR SATELLITE

An Annual Report
for Contract No. NAG-1-1500

to

NASA Langley Research Center
Hampton, Virginia

by

Elaine P. Scott
Assistant Professor

and

Kasey M. Lee
Graduate Research Assistant

Department of Mechanical Engineering
Virginia Polytechnic Institute & State University
Blacksburg, VA 24061-0238

October 10, 1994

PREFACE

In the continuance of this project, it was found that some of the dimensions used for the high-temperature superconductive thermal bridges were incorrect. In addition, an error was detected in the original analysis with the manganin thermal bridges. Consequently, the dimensions of the high-temperature superconductive (HTS) thermal bridges were modified, and the original analysis was redone. These changes indicated some limitations of the computer program SINDA, specifically its inability to converge to the correct temperature distributions for the modified HTS thermal bridge models. Therefore, two versions of the different finite difference program, CONDUCT (two dimensional version, Patankar, 1991, and three dimensional version, Creel and Nelson, 1994), were used. The results in this report reflect the answers obtained by CONDUCT; and, thus, all data referenced by SINDA should be referenced by CONDUCT. However, all the results shown are the updated values found using CONDUCT.

EXPERIMENTAL DESIGN FOR THE EVALUATION OF HIGH-Tc SUPERCONDUCTIVE THERMAL BRIDGES IN A SENSOR SATELLITE

ABSTRACT

Infrared sensor satellites, which consist of cryogenic infrared sensor detectors, electrical instrumentation, and data acquisition systems, are used to monitor the conditions of the Earth's upper atmosphere in order to evaluate its present and future changes. Currently, the electrical instrumentation (connections), which act as thermal bridges between the cryogenic infrared sensor and the significantly warmer data acquisition unit of the sensor satellite system, constitute a significant portion of the heat load on the cryogen. As a part of extending the mission life of the sensor satellite system, the researchers at the National Aeronautics and Space Administration's Langley Research Center (NASA-LaRC) are evaluating the effectiveness of replacing the currently used manganin wires with high-temperature superconductive (HTS) materials as the electrical connections (thermal bridges). In conjunction with the study being conducted at NASA-LaRC, the proposed research is to design a space experiment to determine the thermal savings on a cryogenic subsystem when manganin leads are replaced by HTS leads printed onto a substrate with a low thermal conductivity, and to determine the thermal conductivities of HTS materials. The experiment is designed to compare manganin wires with two different types of superconductors on substrates by determining the heat loss by the thermal bridges and to provide temperature measurements for the estimation of thermal conductivity. A conductive mathematical model has been developed and used as a key tool in the design process and subsequent analysis. The analysis includes studying

the various types of effects, such as the length of the thermal bridge and the heat flux at the warm end of the thermal bridge, on the one-dimensional mathematical models. The results, which were obtained by using the pre-packaged finite difference modeling programs PATRAN (1990) and SINDA (1985), indicate about a minimum of 5 percent heat load by $BiSrCaCu_2O_x$ on Fused Silica substrate and maximum of almost 75 percent heat load by the $YBa_2Cu_3O_7$ on the Green substrate on the cryogen compared to the 20 percent heat load by the currently used manganin wires. The minimum heat load translates to over 15 percent savings on the cryogen and 9 month extension on a 5-year mission. Considering the majority of the HTS materials display heat loads under 15 percent, most of the HTS materials are potential replacements for the manganin wires as the electrical leads because of their ability to decrease the heat load on the cryogen and hence, increase the operational life of the cryogenic infrared detector sensor satellites.

TABLE OF CONTENTS

LIST OF TABLES

LIST OF FIGURES

LIST OF SYMBOLS

A	Cross-sectional area [m^2]
H_c	Critical magnetic field [T]
J_c	Critical current density [A/cm^2]
$K(T)$	Thermal Conductivity [W/m-K]
q''	Heat Flux [W/m^2]
Q	Total heat transfer [W]
S	Objective function (least-squared function)
ΔT	Temperature difference [K]
T_c	Critical or transitional temperature of a superconductor [K]
T_i	Calculated temperatures from SINDA [K]
Y_i	Measured temperatures [K]

LIST OF ABBREVIATIONS

ASTROMAG	Mission name (Wise et al., 1992)
AXAF	Mission name (Wise et al., 1992)
BCS	Bardeen, Cooper, and Schrieffer Theory
BSCCO	$BiSrCaCu_2O_x$
COBE	Cosmic Background Explorer
GLAG	Ginzburg, Laudau, Abrikosov, and Gor'kov Theory
GSFC	Goddard Space Flight Center
HTS	High-Temperature Superconductive
IRAS	Infrared Astronomy Satellite
MIDAS	Materials In Devices As Superconductors
NASA-LaRC	National Aeronautics and Space Administration Langley Research Center
SAFIRE	Spectroscopy of the Atmosphere Using Far-Infrared Emissions
SIRTF	Shuttle Infrared Telescope Facility
SQUID	Superconducting Quantum Interference Devices
YBCO	$YBa_2Cu_3O_{7-x}$
YSZ	Yttrium-stabilized zirconia

CHAPTER 1

Introduction

The purpose of the cryogenic infrared detectors is to monitor the chemical radicals present in the upper atmosphere in order to evaluate the present and future changes in the Earth's environment. The infrared sensor satellites consist of three main systems -- the cryogenic infrared detector, the data acquisition and storage electronics, and the electrical instrumentation, as shown in Figure 1.1. The cryogenic infrared detectors, which are typically made of Mercury Cedium Tellurium (HgCdTe), are used to detect and absorb the radiation due to chemical radicals in the upper atmosphere. These detectors are cooled constantly by a cryogenic refrigeration unit to maintain a temperature in the range of 1.6 to 4 K, depending on the operational requirements of the type of the sensor satellite. The electronic signals representing the radiation data from the sensors are then sent through the electrical instrumentation, specifically the currently used manganin wires, to the data acquisition system for storage. Since the storage unit is kept at a considerably warmer temperature (80 K) than the detector, the electrical leads act as thermal bridges; i.e., they provide an avenue for heat to be transferred to the cryogenic infrared detector.

The mission life of the infrared sensors depends on the amount of cryogen available; i.e., the slower the rate of the cryogen evaporation, the longer the life of the satellite. Therefore, it is of interest to minimize the heat load on the cryogen by any other components besides the heat load due to the radiation caused by the chemical

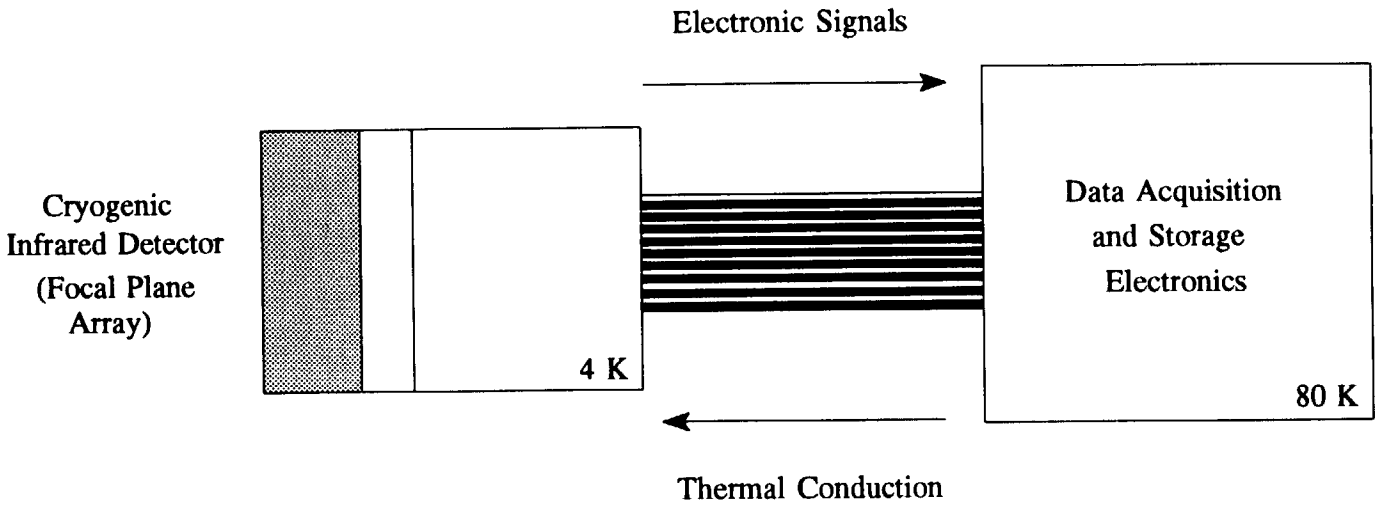

Figure 1.1. Schematic of Infrared Detector Sensor Satellite

radicals striking the detector. Two methods are available for decreasing the nonparasitic heat load on the cryogen: improve the efficiency of the cryogenic refrigeration system, and/or minimize the heat transfer through the electrical instrumentation (leads) to the cryogenic infrared detectors. The present research project is focused on the second method. The four parameters of the electrical leads which can be altered to reduce the thermal transfer to the cryogenic infrared detectors are:

- select materials with low thermal conductance,
- decrease the temperature difference between the ends of the electrical leads,
- minimize the number of electrical connections required,
- increase the physical length of the thermal bridges.

The temperature distribution along the leads depends on the temperatures at the ends of the leads and the thermal properties of the leads. The ends of the leads are fixed at 4 K for the cryogenic infrared detector and at 80 K for the data acquisition and storage systems. Considering that the temperatures of the infrared detector and the data acquisition unit cannot be changed, the temperature difference between the two ends of the electrical leads is fixed. The second option, that of minimizing the number of electrical leads, cannot be exercised because the number of the leads determines the functionality of the cryogenic infrared detector. Unless the infrared detector is changed, the number of the electrical leads must remain the same. Therefore, only two of the available options can be used in the research: using a material with low thermal properties and increasing the physical length of the electrical leads can be used in the research.

Consequently, the Advanced Sensor Systems group of the Electronics Directorate at the National Aeronautics and Space Administration's Langley Research Center (NASA-LaRC) is currently investigating the feasibility of using high-temperature superconductive (HTS) films (leads) printed on low thermal conducting substrate in place of the presently used wires made from manganin, an alloy consisting of 84 percent copper, 12 percent nickel, and 4 percent manganese and having a high thermal conductivity. One of the reasons for the present investigation is that the HTS leads have been discovered to exhibit lower thermal conductivity which translates into lower thermal losses. Concurrently, the HTS materials possess sufficient electrical conductivity for detector applications, where typical currents are on the order of 1 μA. In fact, NASA-LaRC has considered incorporating this technology of HTS materials for future space missions, such as the Shuttle Infrared Telescope Facility (SIRTF), AXAF, and the deep space astronomy mission, ASTROMAG, and the ground mission Spectroscopy of the Atmosphere Using Far-Infrared Emissions (SAFIRE). Preliminary investigations of using HTS materials have indicated a 10 to 15 percent extension on the operational life of these missions based on the total heat load by the electrical instrumentation on the cryogen being at least 20. Therefore, the interest in building similar instruments for other remote sensing missions exists in the future (Wise et al., 1992). One of the first steps that NASA has taken to incorporate the use of the HTS materials was in establishing a program to develop high-temperature superconductive (HTS) materials for NASA-specific applications. At the NASA Goddard Space Flight Center (GSFC), research is being conducted on both bulk material and thin-film applications and has developed the capability to manufacture and

test the materials in-house (Castles et al., 1988). As a result of NASA's investigation in the feasibility study of HTS materials, a spaceflight experiment is being designed to evaluate the use of this superconductive technology in the space environment.

1.1 Goals and Objectives

The goal of this thesis is to design a potential spaceflight experiment in conjunction with NASA's proposal to assess the performance of high-temperature superconductor (HTS) materials in lieu of manganin wires for use as electronic leads in infrared detector sensor satellites (Wise et al., 1992). Based on the goal of this study, two objectives were formulated in designing an experiment for a projected space launch in 1998. The objectives are:

1) quantitatively compare the performance of HTS materials and manganin wires for use as electronic leads to cryogenic sensors, and

2) measure the thermal conductivity of HTS materials.

In order to accomplish these objectives, the experimental design is to consist of at least two identical systems, which differ only in the thermal bridge materials. One system would be manganin and the other(s) would be HTS films printed on low thermal conducting substrate. All other sources of heat transfer such as convection, radiation, and conduction due to other components excluding the thermal bridges in the experiment are to be minimized by the use of radiation shields and vacuum chambers. In addition, the design of the experiment will be constrained by the carrier and sensor satellite requirements. The payload size, power, and weight available for the experiment in the

space shuttle will restrict those parameters in the experimental design. Since a high vibrational load is placed on the experiment during the spaceflight launch, the thermal bridges made of HTS leads need to be mechanically supported because of the brittle nature of the substrate. Manganin wires have been shown in previous spaceflights not to require mechanical supports. Besides the spaceflight requirements, constraints due to the sensor need to be met in designing this experiment. The sensor satellite requires the detector leads to be able to transmit typical signals of 1 μA or less and have current density of 0.05 A/cm^2. Finally, a resource constraint of a $30K budget has been set for the project for economic feasibility.

CHAPTER 2

Literature Review

This section contains the chronological development of the different types of superconductors and the application of high-temperature superconductors (HTS) and discusses the issues important in the application of HTS materials in various technological fields, especially in space.

2.1 Development of Applied Superconductivity

Application of superconductivity was not considered possible until the 1950's and the 1960's. In fact, actual applications of high-temperature superconductors did not become feasible until the mid-1980's. Before then, the discovery and development of the theory of superconductors occupied the scientists, physicians, and engineers of this field.

2.1.1 Discovery of Low-Temperature (Type I) Superconductors

Superconductivity was first observed in mercury by Professor Heike Kamerlingh Onnes at the University of Leiden in 1911. He was examining the contemporary view that the electrical resistance of metals has two components, one due to the scattering of the conduction electrons by the thermal vibrations of the metallic atoms, and one due to their scattering by the impurities in the metal. The first component was expected to decrease continuously with falling temperature and vanish at 0 K. The second was

regarded as essentially independent of temperature (Hunt, 1989). Therefore, Kamerlingh Onnes was interested in observing how small a resistance mercury could attain at liquid helium temperature. The reason for choosing mercury was that a relatively high purity of mercury was easily attained (Nagamiya, 1969). His work showed that the resistivity, instead of decreasing continuously with falling temperature, disappeared sharply at 4.15 K, and that this behavior was not greatly altered by the presence of impurities. Hence, the existence of a new state of mercury characterized by the absence of electrical resistivity came to be recognized, and to be known as the "superconducting" state (Allen, 1969). As a result of his study, Kamerlingh Onnes discovered the transition temperature (T_c) which is the maximum temperature at which superconductivity can exist without being destroyed (Allen, 1969). The superconductors discovered during this time were distinguished as 'Ideal', 'Type I', or 'soft' superconductors. Type I superconductors are usually a certain type of metal, particularly those that have low melting points and are mechanically soft and easily obtained in pure, strain-free conditions (Allen,1969).

Kamerlingh Onnes showed that a superconductor is a perfect conductor, but Meissner and Ochsenfeld (1933) showed that a superconductor has very interesting magnetic properties. The superconducting state possessed the entirely independent property of excluding magnetic flux completely, except in the neighborhood of the surface. For instance, if a superconductor is approached by a magnetic field, screening currents are set up on its surface. These screening currents create an equal but opposite magnetic effect, thereby canceling the magnetic field and leaving a net magnetic field of zero inside the superconductor. This phenomenon is known as the "Meissner Effect".

The Meissner Effect occurs only if the magnetic field is relatively small. If the magnetic field becomes too great and exceeds the critical magnetic field (H_c), a characteristic of the superconducting material, it penetrates the interior of the metal and thereby destroys its superconductivity (Hunt, 1989).

The theory of Type I superconductors has been derived and validated by Bardeen, Cooper and Schrieffer (1957). The theory of Bardeen, Cooper, and Schrieffer (BCS theory) defined that the interaction between electrons and phonons (vibrational modes in the lattice of atoms making up the material) leads to a pairing of electrons. The electrons, which normally repel each other, develop a mutual attraction and form twosomes called Cooper pairs. At low temperatures, these so-called Cooper pairs condense into an electrical superfluid, with energy levels a discrete amount below those of normal electron states (known as the superconducting energy gap). According to Schrieffer, "all the electrons condense into a single state, and they flow as a totally frictionless fluid." (Hunt, 1989).

2.1.2 Discovery of High-Temperature Superconductors

Soon after Meissner, a Russian physicist, Schubnikov (1937) found that some superconductors seem to allow flux penetration. When the applied magnetic field is above a lower critical field, called H_{c1}, the flux begins to penetrate but the material remains superconducting until a higher critical field, the upper critical field, H_{c2} is reached. The materials which displayed this type of behavior were named as "Type II Superconductors", distinguishing from the "Type I" superconductors discovered earlier

(Bardeen, 1968).

In Type II superconductors, the flux is penetrated by means of quantized vortex lines about which electrons circulate and give rise to a magnetic field. Abrikosov (1953) worked out his now famous theory of Type II superconductors based on flux penetration in the form of an array of quantized vortex lines. The basis of the earlier understanding of Type II superconductors is the theory of Ginzburg, Laudau, Abrikosov, and Gor'kov, also known as GLAG theory (Bardeen, 1968). There is no confirmation if the phenomenon of the Type II superconductors currently discovered is explained by the GLAG theory.

Eventually, the interest in superconductivity gradually declined until Alex Mueller and Georg Bednorz, scientists at the IBM Zurich Laboratory, sparked the recent excitement in 1986. They had spent much of 1984 and 1985 looking for high T_c superconductivity in a class of metal oxide ceramic materials called perovskites. In January of 1986, they found indications of superconductivity at approximately 30 K in barium lanthanum copper oxide (Hunt, 1989). This superconducting phase was soon identified as the compound $La_{2-x}Ba_xCuO_4$ at the University of Tokyo and elsewhere. Towards the end of 1986, T_c was elevated to 40 K by replacing barium with strontium in this formula (Geballe and Hulm, 1988).

Early in 1987, Chu and his associates found superconductivity near 95 K in a mixed phase sample containing yttrium, barium, copper, and oxygen. This superconductor was identified as $YBa_2Cu_3O_7$. However, this sudden advance from 23 K to 95 K in superconductors was not only unpredicted by theory, but appears to be beyond the

capability of the GLAG theory to explain. The known stable Type II superconductors up to now are $YBa_2Cu_3O_7$ and $BiSrCaCu_2O_y$ (BSCCO). The BSCCO oxide has T_c of about 105 K, being higher than that of $YBa_2Cu_3O_7$ by more than 10 K (Maeda et al., 1988).

2.2 High-Temperature (Type II) Superconductors

High-temperature superconductors, also known as Type II superconductors, are a type of superconductor with two critical magnetic fields. They allow flux penetration when the applied magnetic field exceeds the first critical magnetic field, H_{c1}, and the superconductivity of the material is not destroyed until the magnetic field exceeds the second critical magnetic field, H_{c2}. The following describes in details the characteristics and the structure of HTS materials.

2.2.1 HTS Materials Characteristics

A larger number of so-called high-temperature superconductors are now known to exist in two basic types (the so-called 40 K and the 95 K [for 1-2-3] materials) and more recently, $BiSrCaCu_2O_x$. The $YBa_2Cu_3O_{7-x}$, so-called 1-2-3, compounds are highly sensitive to oxygen content, changing from semiconducting, at $YBa_2Cu_3O_{6.5}$ to superconducting at near $YBa_2Cu_3O_7$, without losing their crystalline integrity (Geballe and Hulm, 1988). To date, this material has been synthesized in polycrystalline bulk and oriented thin-film forms; high-temperature superconductivity has been observed in these materials only when the oxygen content is seven oxygen atoms per molecule (x=2) (Iafrate, 1988). The high sensitivity of their properties to oxygen content is due to the

apparent ease with which oxygen can move in and out of the molecular lattice (Hunt, 1989). Surprisingly, the substitution of the other rare earths, even magnetic ones, for yttrium in the 95 K compounds results in very little change in superconducting properties, such as the critical temperature T_c (Geballe and Hulm, 1988). More recently, copper-oxide ceramics containing bismuth or thallium have been found, known as $BiSrCaCu_2O_x$ (BSCCO), with the critical temperatures in the range, respectively, of 110 K and 125 K (Hunt, 1989). The BSCCO material is formed from a rare-earth material similar to the YBCO, but BSCCO materials have slightly different superconductive properties, such as T_c, J_c, and H_c. The differences in the superconductive properties for these two types of rare earth materials are provided in more details in the following sections.

2.2.1.1 $YBa_2Cu_3O_7$ Properties

$YBa_2Cu_3O_7$ samples generally exhibit extremely high upper critical fields. Preliminary measurements indicate that for single crystals, H_{c2} is anisotropic; that is, it is dependent upon field direction relative to the a-, b-, or c-axes of the orthorhombic lattice shown in Figure 2 (Choi et al., 1992). Values for H_{c2} for 1-2-3 phase ranging from 30 tesla [T] (c-axis) to 150 T (a- or b-axes) are reported at 4.2 K (Hunt, 1989). The tesla is a SI unit (1 N/(C-m/2)) for measuring the magnetic field. At 0 K, H_{c2} is estimated to be between 80 and 180 T in the Y-Ba-Cu-O system investigated (Wu et al., 1987).

Due to the anisotropic characteristics, the 1-2-3 ceramics show differences of as much as 30:1 in the critical current density (J_c), which is the maximum amount of

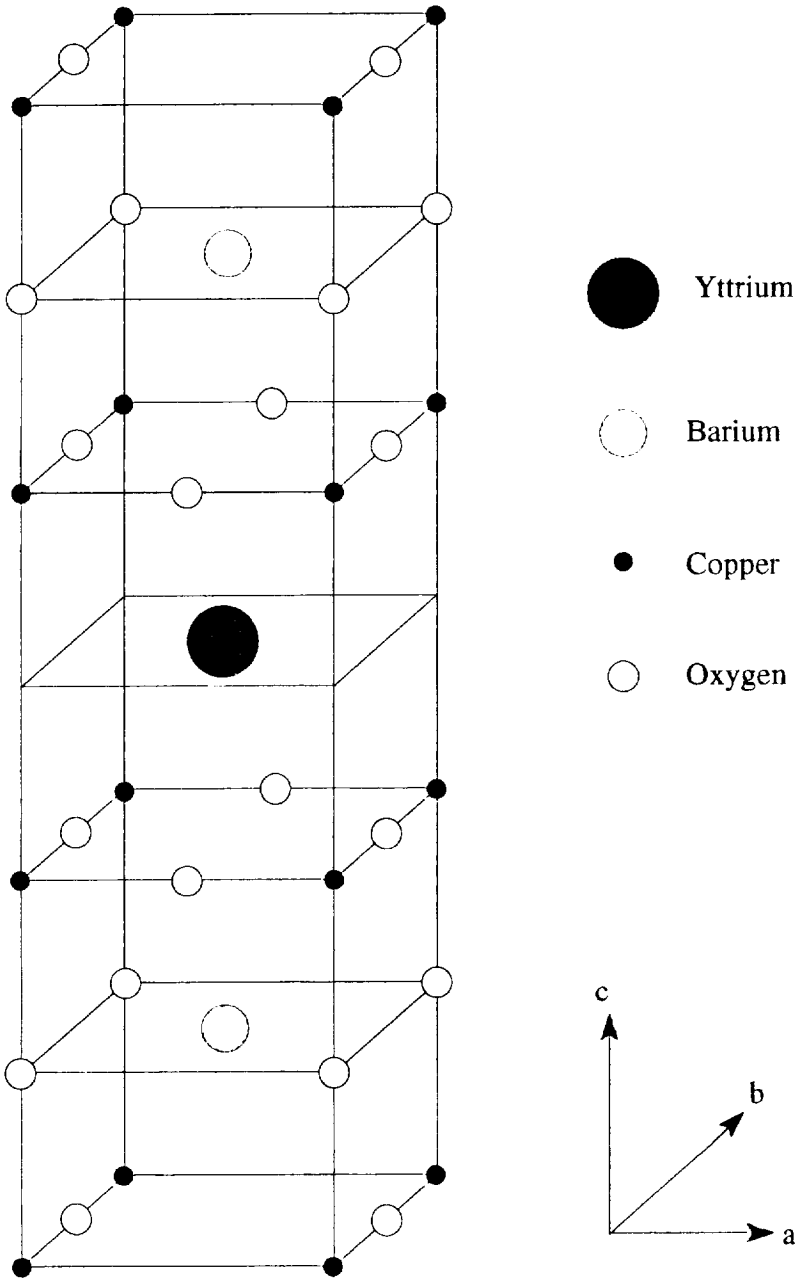

Figure 2.1. Orthorhombic Strucutre of YBCO Unit Cell

electricity allowed to flow through a given per area, depending on grain orientation. The grain boundaries seem to be the primary culprit for the current density limitations rather than the anisotropy (Hunt, 1989). The grain boundaries, for example, may be regions where the superconductivity is degraded, and such weak links can dominate the behavior (Geballe and Hulm, 1988). In zero applied magnetic field, the highest J_c reported at 77 K for bulk polycrystalline $YBa_2Cu_3O_{7-x}$ materials is about 10^3 A/cm^2, with J_c values in the range of 200 A/cm^2 being more usual (Ekin et al., 1987)

2.2.1.2 $BiSrCaCu_2O_x$ Properties

At zero magnetic field, the majority of transitions for the BSCCO superconductor occured above 103 K, with the onset transition temperature being 115 K. The critical current density for the $BiSrCaCu_2O_x$ sample is 0.6 mA/cm^2 at 100 K, which is very small compared to YBCO (Kumakura et al., 1988). The BSCCO materials are more limited in their applicability because of the lower critical current density; i.e. the YBCO can be used in more applications. Also for BSCCO phase, the second critical magnetic field (H_{c2}) at 77 K, estimated from a linear extrapolation, is 41 T and 245 T for the midpoint of the transition resistivity. These H_{c2} values are about twice as large as those for the Ba-Y-Cu-O system. This is due to a larger temperature difference between T_c and the liquid nitrogen temperature (T_c = 77 K) in the BSCCO system. The H_{c1} of BSCCO is about 4.5 mT at 77 K. This H_{c1} value is much smaller than that of the Ba-Y-Cu-O compound (Kumakura et al., 1988).

2.2.2 High-Temperature Superconductor Structure

The Type II superconductors occur in at least two crystalline forms which are closely related to the perovskite structure, ABO_3. The common feature of these compounds are the sheets of Cu-O bonds. The first new superconductor of Type II, $La_{1.85}Sr_{0.15}CuO_4$ ($T_c \approx 40$ K) was derived by doping the parent compound La_2CuO_4 (the so-called 214 phase) which occurs in the tetragonal K_2NiF_4 structure type. The superconductivity of the second remarkable class of oxide superconductors, typified by $YBa_2Cu_3O_7$ (YBCO) ($T_c \approx 95$ K), the so-called 123 phase and $BiSrCaCu_2O_x$, are not derived by metallic doping, as in the 214 phase (Geballe and Hulm, 1988).

2.3 Application of High-Temperature Superconductors

The theoretical basis for electronic applications did not appear until 1962. Brian Josephson, then a graduate student at Cambridge University, analyzed what would happen at the intersection of two superconductors separated by a thin insulating barrier (now called a Josephson Junction). He predicted that a supercurrent would tunnel right through the barrier and that there would be no voltage across the barrier as long as the supercurrent did not exceed a critical value. He also predicted that a voltage across the barrier would create a high-frequency alternating supercurrent. His predictions defied common sense and they evoked considerable skepticism, but John Rowell, Phil Anderson, and S. Shapiro verified them experimentally in 1963 (Hunt, 1989).

However, the flurry of activity in application did not occur until the late 1980's. A rule of thumb for general applications is that materials must be operated at a

temperature of 3/4 T_c or below. At about 3/4 T_c, critical fields have reached roughly half their low-temperature limit, and critical current densities roughly a quarter of their limit. Thus, to operate at liquid nitrogen temperature (77 K), one would like T_c near 100 K, making the 95 K material just sufficient (Hunt, 1989). Since the HTS materials with T_c near 100 K were not discovered until the late 1980's, the application of the HTS materials has only recently been feasible.

2.3.1 Areas of Application of High-Temperature Superconductors

Applications of superconductivity have spanned a wide range of technical areas; geophysics, high-energy physics, materials science and medicine, to name a few (Geballe and Hulm, 1988). Near-term prospects for high-temperature superconductivity applications include magnetic shielding, the voltage standard, Superconducting Quantum Interference Devices (SQUID), infrared sensors, microwave devices, and analog signal processing (Hrovat et al., 1992). Longer-term prospects include large-scale applications such as microwave cavities; power transmission lines; and superconducting magnets in generators, energy storage devices, particle accelerators, rotating machinery, medical imaging systems, levitated vehicles, and magnetic separators. In electronics, long-term prospects include computer applications with semiconducting superconducting hybrids, Josephson devices, or novel transistor-like superconducting devices. Several of these technologies will have military applications (Hunt, 1989).

In each application, it is the capability for vastly improved performance or the ability to perform tasks which were not previously feasible which is the incentive for the

use of superconductivity (Geballe and Hulm, 1988). Areas where the best possible noise performance is desired are in space applications of microwave and infrared detectors centering on radio and infrared astronomy and on communications (Sullivan and Vorreiter, 1979). In fact, the use of HTS materials for sensor leads for several sensing systems in millimeter and infrared ranges will provide better noise isolation and focal plane thermal isolation; i.e., the ceramic superconductors provides the ability to thermally isolate one spacecraft system from another while reducing the electrical losses. In addition, the incorporation of HTS materials ensures a reduced cryogenic requirement and higher-frequency operation (Krishen and Ignatiev, 1988).

2.3.2 Requirements for Using HTS Materials

There are two major issues which need to be resolved before viable applications of HTS materials can be realized. The first, the materials issue, concerns the processing requirements; i.e., the synthesis of stable, reproducible materials with useable electromagnetic properties and current densities. It is not obvious at the present time, for example, whether the oxygen stoichiometry and ordering can be controlled well enough at the critical surfaces and interfaces to make reliable devices with predictable characteristics. Chemical stability is also limited because oxygen leaves the structure under vacuum, even at room temperature. Superface protection techniques need to be developed to allow satisfactory performance and lifetime of the materials under various conditions of storage and operation. These concerns are heightened in thin films, in which, for some applications, the chemical composition of the outer atomic layers need

the surface to be maintained through many processing steps, and in which diffusion into the substrate interface could degrade super-conducting properties (Hunt, 1989). The second, the concepts issue, involves the elucidation of fundamental physical limitations inherent in the phenomena of high-temperature superconductivity. It is not obvious whether the outstanding signal-to-noise characteristics, which make the presently used sensors that operate at 4 K so desirable, will be sufficiently good if the operating temperature is raised to 77 K (Iafrate, 1988).

2.3.3 Processing of HTS Films

Ever since the discovery of HTS, the utilization of superconductors as thin films has become possible. Over the past years, many different deposition techniques have been studied in creating thin films, including electron beam evaporation, sputtering, molecular beam epitaxy, laser evaporation, and metalorganic deposition (Aslam, et al., 1988).

However, there are very few processes by which thin films have been proven to be effective because of the problem of fabricating thin or thick films of high-temperature superconductors on dielectric substrates (Hunt, 1989). The most apparent aspect of the problem is the chemical degradation of the film, specifically a decrease in the temperature for zero resistivity (Cima et al., 1988). The following discussion considers the most popular and feasible method, screen printing, because HTS films by the screen printing process yield the materials with the higher T_c's widely necessary for the processing of electronic devices (Koinuma et al., 1987).

Screen printing is a relatively simple method which has been explored by NASA and by others. Reports from NASA focus on the strong influence of the substrate material on the characteristics of the screen-printed $YBa_2Cu_3O_{7-\delta}$ films (Bansal et al., 1988). In order to apply screen-printed thick films to electronic devices, it is necessary to produce thick films with strong c-axis orientation to obtain a high critical current density (Tabuchi and Utsumi, 1988).

One way of producing screen-printed HTS leads on substrate is to begin by preparing the powders with nominal compositions of $(Yb_{0.25}Ba_{0.75})_3Cu_3O_{9-\delta}$ (powder A) and $(Yb_{0.32}Ba_{0.68})_3Cu_3O_{9-\delta}$ (powder B) by mixing the prescribed amounts of Yb_2O_3, $BaCO_3$, and CuO in ethanol, calcining the dried mixture at 900 °C for 12 h, pulverizing the calcined product, and further calcining the powder at 900 °C for 2 h (powder A) or at 900 °C for 2 days (powder B). Yb-Ba-Cu-O paste is prepared by mixing the powder and hepthyl alcohol in an agate mortar and is printed on several kinds of substrate (quartz, alumina, yttrium-stabilized zirconia (YSZ), and La_2CuO_4) through a 150 mesh silk screen. After drying in vacuo at 150 °C for more than 6 h, the printed films are sintered in air at 900 °C for 0.5 to 5 h (Koinuma et al., 1987).

Most results show that the superconducting transition temperature, surface smoothness, resistivity, crystal structure, and adhesion of these films are highly sensitive to the post-printing heat treatment in the screen printing method. Highly adherent and smooth films, which attain a zero state at 79 K, have been synthesized by optimizing the annealing conditions (Budhani et al., 1987).

2.3.4 Possible Substrates for Applications

There are basically four known dielectric substrate material candidates: fused silica (SiO_2), Yttrium-Stabilized Zirconia (YSZ), Alumina (Al_2O_3), and Magnesia (MgO). The superconductors printed on fused silica and YSZ prove to be superconducting, but when printed on alumina and magnesia, YBCO and BSCCO prove to be insulators (Wise et al., 1992).

Although YSZ's dielectric behavior does not suit many electronic applications, its refractory nature has led many to believe that its chemical interactions may be sufficiently slow to allow extended thermal treatment of deposited films without significant chemical degradation. YSZ, however, is not completely inert to Barium-Yttrium-Copper (BYC): degradation manifests itself as a lower critical temperature for BYC films on YSZ substrates. Cima et al. (1988) describe results of experiments indicating the chemical reactions by which BYC films degrade on YSZ substrates.

These results indicate that the BYC completely decomposes to $BaZrO_3$ in the presence of ZrO_2. The overall chemical reaction can be represented as:

$$2Ba_2YCu_3O_{6.5}+4ZrO_2 \rightarrow 4BaZrO_3+4CuO+Y_2Cu_2O_5 \qquad (1)$$

The driving force for this reaction is provided by the high chemical stability of $BaZrO_3$. The reaction between BYC and YSZ thus appears to proceed by barium removal from BYC, yielding yttrium- and copper-rich material. If local thermodynamic equilibrium in the film is maintained throughout this process, the extraction proceeds with

the formation of CuO and a transient appearance of BaY_2CuO_5 (211 or Green Phase) followed by $Y_2Cu_2O_5$ formation. Thus, the primary degradation mechanism involves barium loss from the film rather than film contamination by substrate material (Cima, et al., 1988). Since BaY_2CuO_5 (211 Phase) is a compound which is stable, it is a possible substrate candidate (Cima et al., 1988).

Typically, films deposited directly on SiO_2 show very broad transitions with T_c below 40 K for SiO_2 substrates. Studies suggest that the poor quality of these films is due to the severe interaction between the films and the SiO_2 substrate (Aslam et al., 1988). Buffer layers help to overcome strong substrate reactions, with especially favorable combinations being ZrO_2/Ag and MgO/Nb (Gurvitch and Fiory, 1987). Several research groups have investigated the use of a buffer layer (e.g., ZrO_2, and Ag) between the YBaCuO films and the SiO_2 substrate to suppress the diffusional effects. The most successful results appear to be those obtained by Mogro-Campero and Turner (1988), who very recently reported T_c = 83 K for furnace-annealed films on SiO_2/Si substrates with a ZrO_2 buffer layer (Aslam et al., 1988).

CHAPTER 3

Experimental Plan

In order to accomplish the objectives and goals of this thesis, an experimental design is needed to accurately mimic the thermal conditions of actual sensor satellites. Therefore, the experimental design was formulated to follow a strategic plan containing the following:

- A liquid-helium temperature of 4 K at one end of the thermal bridge corresponding to the temperature of the cryogenic infrared detector,
- A temperature of 80 K at the warm end of the thermal bridge corresponding to the temperature of the data acquisition and storage system,
- A measurable heat flux to maintain the temperature at the warm end,
- The minimization of all other modes of heat transfer, including convection, radiation, and conduction through any other components excluding the thermal bridges, and
- The capability of withstanding the vibrational loads associated with the spaceflight launch.
- A means of quantitatively comparing different types of thermal bridges

The remaining subsections contain the description of the overall preliminary design as well as the details of the thermal bridges and the method used to perform the thermal conductivity measurements.

3.1 Preliminary Design of the Experiment

The preliminary design of the experiment, shown as Figure 3.1, has been completed. There are basically three major components: the liquid helium dewar, the cryostat, and three identical vacuum chambers which contain three different types of electronic lead (thermal bridges). For operation on the shuttle flight, there are weight and power limitations of 91 kg and 200 W, respectively. The experimental design meets these requirements because the estimated weight and power are 50 kg and 40 W, respectively. The remaining subsections describe in detail the specific components of the experimental design. These components were designed using some of the same ideas incorporated in the future space experiment satellite, MIDAS. MIDAS, which NASA is currently completing, is the first experiment that will test and use the HTS materials as possible electrical connections in space.

3.1.1 Details of the Cryogenic Refrigeration System

The cryogenic cooling concept, which incorporates a liquid helium dewar, is used in several infrared mission satellites such as the Infrared Astronomy Satellite (IRAS), the Cosmic Background Explorer (Cobe) mission (Volz et al., 1990), and the Shuttle Infrared Telescope Facility (SIRTF) (Lee, 1990; Sherman, 1983). It has been used as a basis for this experimental design. This experimental design, however, has an additional component in the cooling system, the cryostat shown in detail in Figure 3.2. The liquid helium from the dewar is fed to the cold tip of the thermal bridges in the vacuum chambers by way of an open-cycled cryostat. The open-cycled cryostat is the Heli-tran

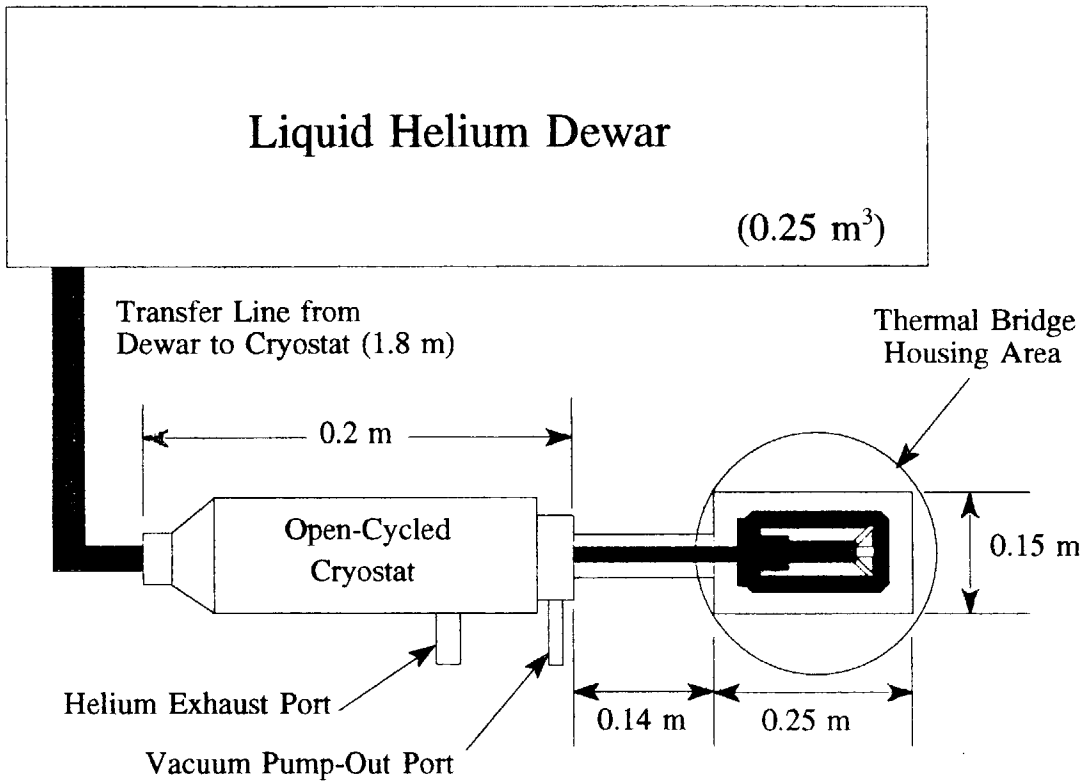

Note: Drawing is not to scale.
Dimensions are preliminary.

Figure 3.1. Preliminary Thermal Bridge Experimental Design

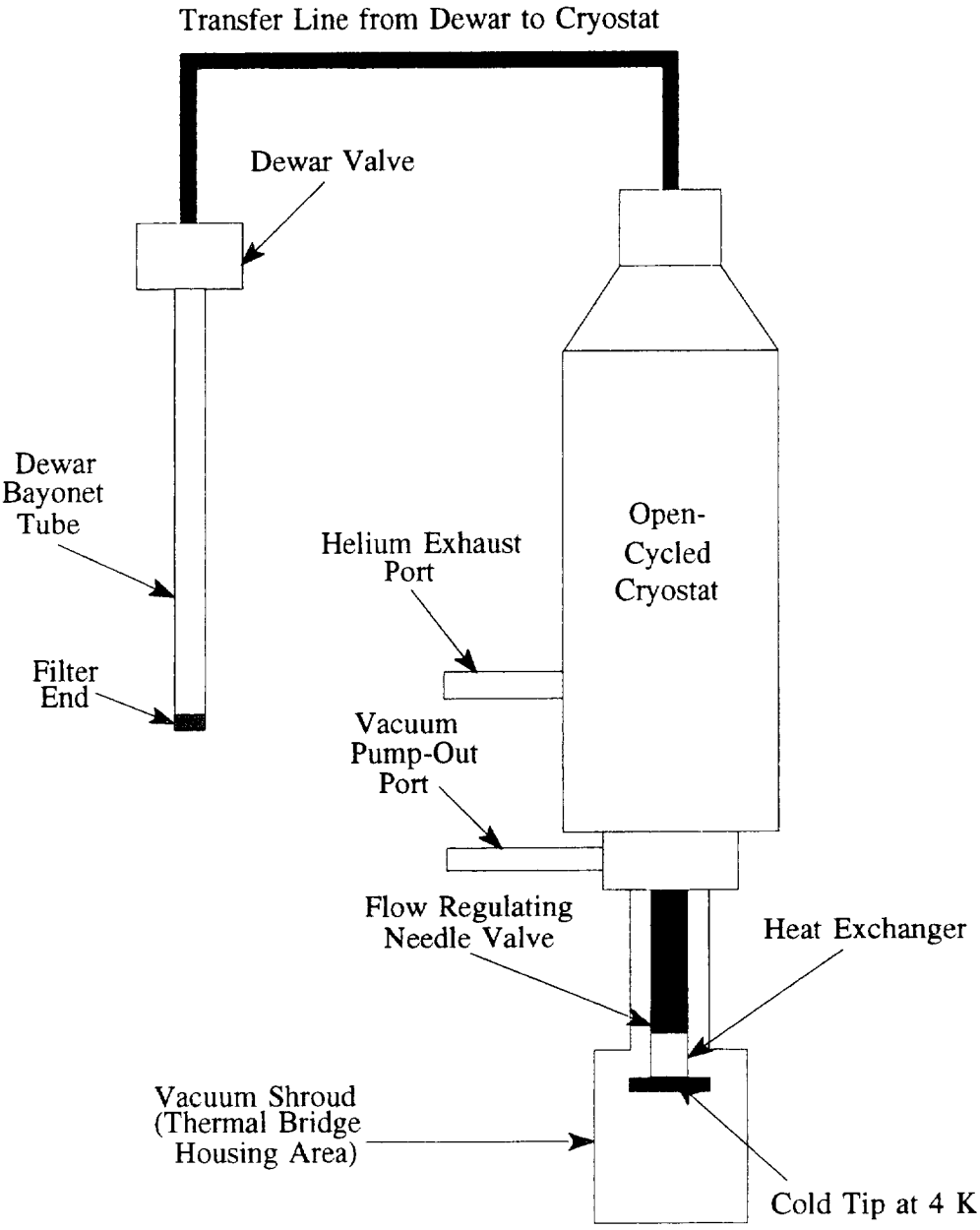

Figure 3.2. Detailed View of the Heli-Tran LT-3-110

LT-3-110 model from APD Cryogenics Inc. The function of the cryostat involves an external pressure source forcing the cryogen out of the storage dewar and through the transfer line's flow-regulating needle valve to the cold end. A filter in the dewar bayonet end screens out foreign matter. The transfer line's patented internal-suspension system and independent shielding circuit minimize heat leak of the cryogen as it flows through the line. In the LT-3 cold end, flow through a heat exchanger serves as the conductive-cooling interface for the sample holder. The sample holder is enclosed in a vacuum shroud which in the experimental design is the thermal bridge housing area. This vacuum shroud seals with the cold end via high-vacuum O-ring seals. The cold end and vacuum shroud are easily rotated in any orientation during operation. After cooling the sample, the helium — now a gas — conductively cools the radiation shield before leaving the cold end. This exhausting gas is heated to prevent cryogenic burns and frost buildup on the cold end and vacuum shroud.

3.1.2 Details of the Thermal Bridge Housing Area

The thermal bridge housing area (vacuum shroud) of the cryostat serves as the holding place for the thermal bridges. A cross-sectional view of the three identical vacuum chambers, which only differ in the material type, is provided as Figure 3.3. The details of the HTS thermal bridge housing area is provided as Figure 3.4. A vacuum environment of 6.8×10^{-6} atm exists in the chambers to minimize the convective losses. The thermal bridges are encased in an area surrounded by radiation shields to minimize the losses due to radiation. As seen in Figure 3.4, the thermal bridges are held between

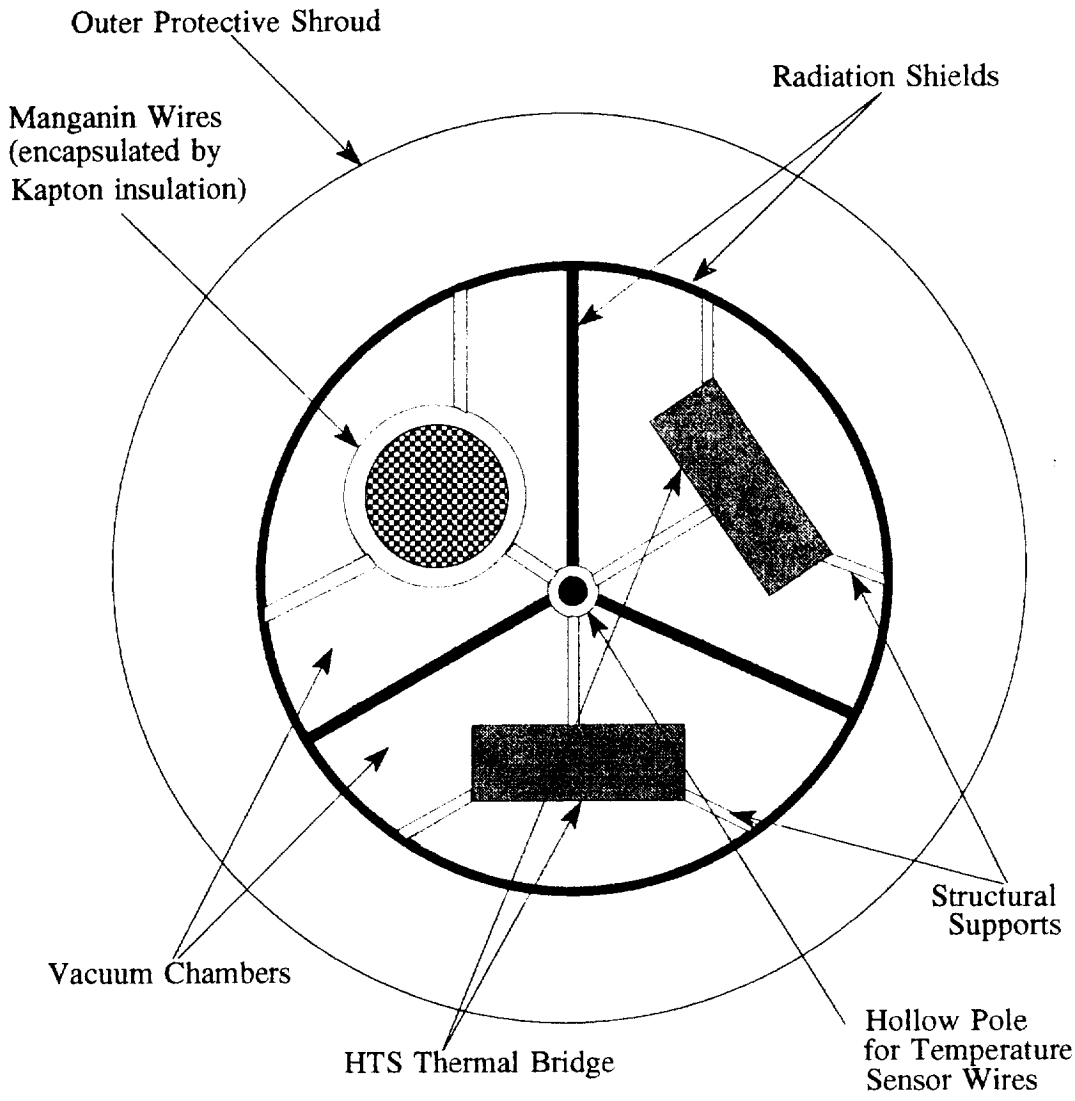

Figure 3.3. Cross-Sectional View of Thermal Bridge Housing Area

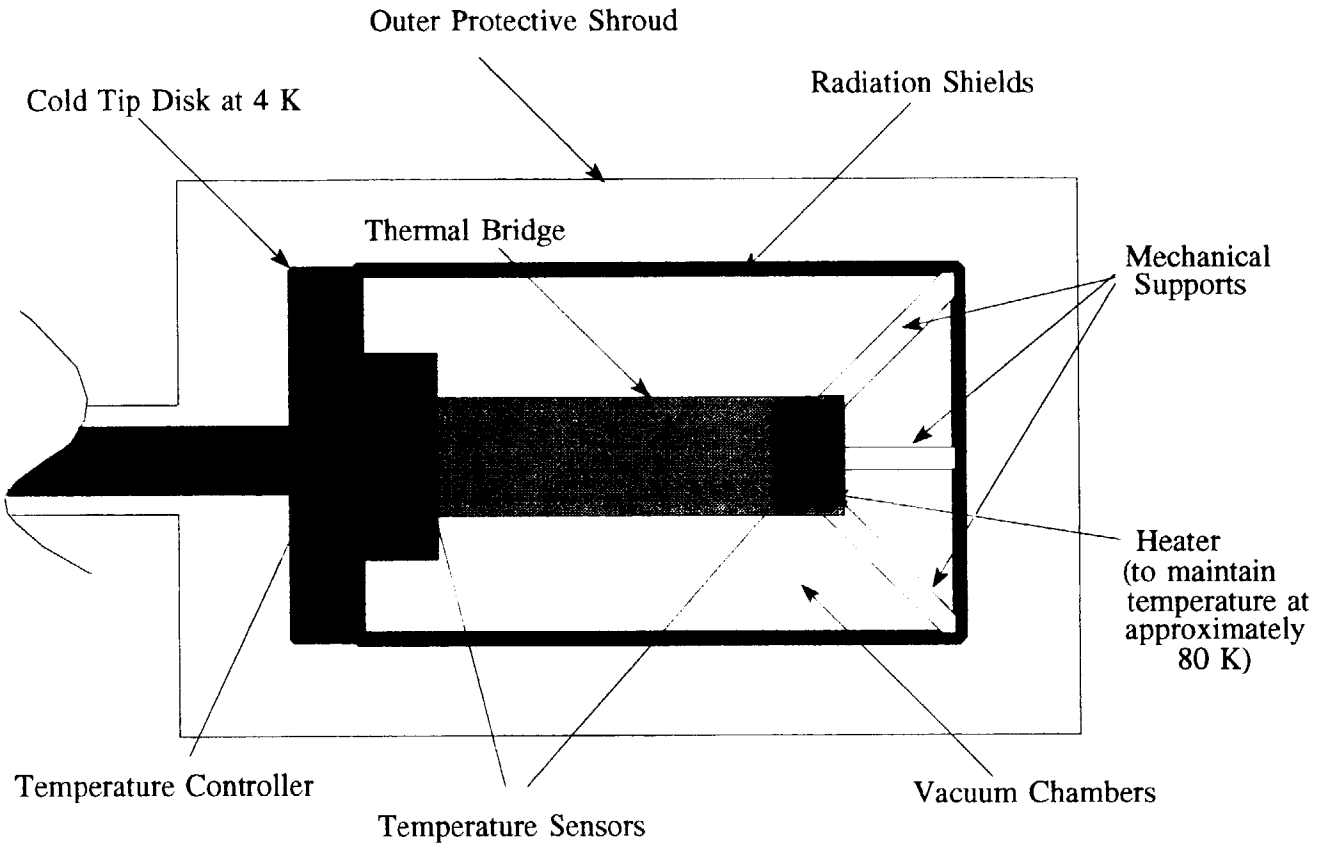

Figure 3.4. Detailed View of the Thermal Bridge Housing Area

a steady heat flux controlled by a heater at one end to maintain an approximate temperature of 80 K and at the other end by a copper block. The copper is in direct contact with a cryogenically cooled disk controlled by a temperature controller to provide a steady, fixed temperature of 4 K. A suggested temperature controller to be used is Model 9600-1 SI Instrument digital temperature indicator/controller from APD Cryogenics Inc., which is a single-channel device.

The experimental set-up provides a method to calculate the heat loss due to the various types of thermal bridges, which is one of the objectives of the research. The heat loss can be determined by calculating the heat transfer through the copper block using simple conduction analysis. In order to perform the analysis, the temperature gradient across the copper block and the thermal conductivity and dimensions of the copper block need to be known. The only unknown variable is the temperature at the end of the copper block which is in contact with the thermal bridge. One way to measure this temperature is through the use of a temperature sensor. The experimental design requires two temperature sensors for each thermal bridge, which is a total of six temperature sensor indicators for all the thermal bridges, since the temperatures at both ends of the thermal bridge need to be determined. Digital temperature indicators are available with four and eight channels. Therefore, the model series 9300 with eight channels will be selecte, since the experiment requires a minimum of six channels. The two extra sensors will be used to monitor the temperature of the radiation shields. The temperature sensors used for the experiment will be Model Si-410 silicon diode thermometer Group AA (APD Cryogenics Inc.) which provides an accuracy of ± 0.1 K from 1.5 to 25 K, which meets

the requirement of providing a steady fixed temperature at the cold end. The temperature readings will be taken from the sensors via wires which are routed through the hollow center pole as shown in Figure 3.3. This hollow pole is to be made from the same type of material used in the mechanical supports to minimize conduction losses. The losses through the sensor wires and the mechanical supports will be included in future work pertaining to this project.

3.1.3 Spaceflight Requirements

Finally, the design of the experiment needs to meet the requirement of surviving the vibrational loads of 12.6 g rms during the space launch. The manganin wires have already been qualified in actual spaceflight missions and do not require additional structural supports. However, the HTS leads on the substrate do require structural supports because of their brittle nature.

A preliminary structural analysis has been performed by Becky A. Spencer, an undergraduate student in the Department of Engineering Science Mechanics at Virginia Polytechnic Institute and State University (VPI & SU). In the structural analysis, several support mechanisms have been considered and studied. Although there is no specific support design for the experiment, there are specific requirements set for the support mechanisms in respect to the experimental design. For instance, the material for the mechanical supports is chosen to be G-10CR which is a material that retains its properties at cryogenic conditions. Secondly, the supports are fixed to the sides of the vacuum chambers. For the actual spaceflight, NASA will be performing a complete structural

analysis to qualify the experiment for launch.

3.1.4 Determination of Thermal Conductivity

The experimental design includes the capability to determine the temperature distributions along the thermal bridges and hence, the measurement of the thermal conductivity of the HTS materials. The analysis for the estimation of the thermal conductivity is beyond the scope of this thesis; however, a brief description of the process is given here. The Box-Kanemasu method, using the experimental and analytical temperature distributions of the HTS materials, is implemented to determine the thermal conductivity of these materials. The Box-Kanemasu method is based on the minimization of an objective function, specifically the least squares functions which include both the experimental and the analytical temperatures. The objective function equation is

$$S=\sum_{i}^{n} (Y_i-T_i)^2, \tag{2}$$

where Y_i are the measured temperatures, T_i are the calculated temperatures, and S is the objective function. The thermal conductivity is a function of temperature and can be represented by:

$$K(T)=a_0+a_1T+a_2T^2+...+a_nT^n. \tag{3}$$

The purpose of the method is to minimize the objective function with respect to the unknown parameters a_0, a_1,..., a_n. One approach to do this is to differentiate Eqn (2) with respect to each of the unknown parameters, set the resulting expressions equal to zero, and then solve for the unknown values. Box-Kanemasu method is an iterative

scheme to perform this minimization procedure. Details of the procedure are given by Beck and Arnold (1977).

3.1.5 Materials

The materials used for the experiment are the manganin wires and the HTS films printed on a ceramic type substrate. There are five possible superconductor/substrate combinations: $YBa_2Cu_3O_{7-x}$ lines on yttria-stabilized zirconia (YSZ, 10wt%, cubic); $BiSrCaCu_2O_x$ lines on YSZ; $YBa_2Cu_3O_{7-x}$ lines on fused silica (3000 Å buffer layer of zirconia); $BiSrCaCu_2O_x$ lines on fused silica (3000 Å buffer layer of zirconia); and $YBa_2Cu_3O_{7-x}$ lines on 211 (Green) Phase.

In the case of fused silica, a buffer layer of zirconia (ZrO_2) is deposited onto the fused silica substrate prior to printing of the superconductor lines to prevent chemical reaction and to alleviate the thermal expansion mismatches between the superconducting material and the substrate. This layer is deposited by reactive sputtering of zirconium metal in a Ar/O_2 atmosphere in an approximate thickness of 3000 Å (a conservative number).

In general, the superconductor/substrate thermal bridge is prepared by depositing HTS materials on the substrate by screen-printing from superconductive pastes. The superconductive powder is prepared by NASA in-house, mixed with a proprietary solution paste (Dupont), and the paste is then screened by a silk mesh using a traditional printer. The selection of the substrate was based on NASA research in which the thermal calculations showed that the superconductive leads printed onto YSZ and fused silica

substrates significantly reduced the thermal load on the liquid helium dewar (Wise et al., 1992).

Since there are only three chambers available within the experimental design, only two of the five combinations of the HTS materials and the manganin model will be selected for the actual spaceflight. However, for the present the analysis will include all the materials.

3.1.6 Dimensions of the Thermal Bridges

Each thermal bridge contains a minimum of 60 detector leads; this set value is used to ensure that the electrical leads meet the electrical requirement of a cryogenic infrared detector which typically transmits signals of 1 μA or less. In the case of manganin, these are 40 AWG wires encased in a thin layer of Kapton insulation (about 0.0254 mm thickness or less). In the case of HTS materials, the superconductors are 60 HTS leads printed onto a 152.4 mm long by 9.144 mm wide by 0.1524 mm thick substrate as seen in Figure 3.5. Each HTS lead is 0.0508 mm wide by 0.0508 mm thick. The spacing between the leads is 0.1016 mm. Details of HTS dimensions are shown on Figure 3.6.

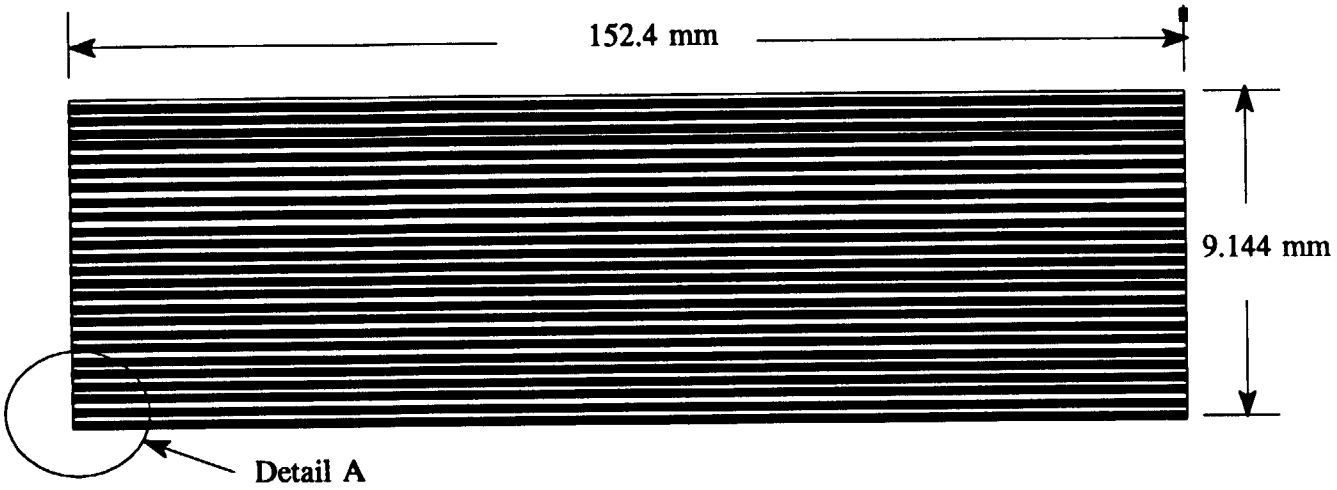

Legend: High Temperature Superconducting Leads

Substrate Material

Notes: 1. Not to Scale.
2. 60 HTS leads are printed on a substrate

Figure 3.5. High Temperature Superconducting Leads Printed on Substrate (Thermal Bridge)

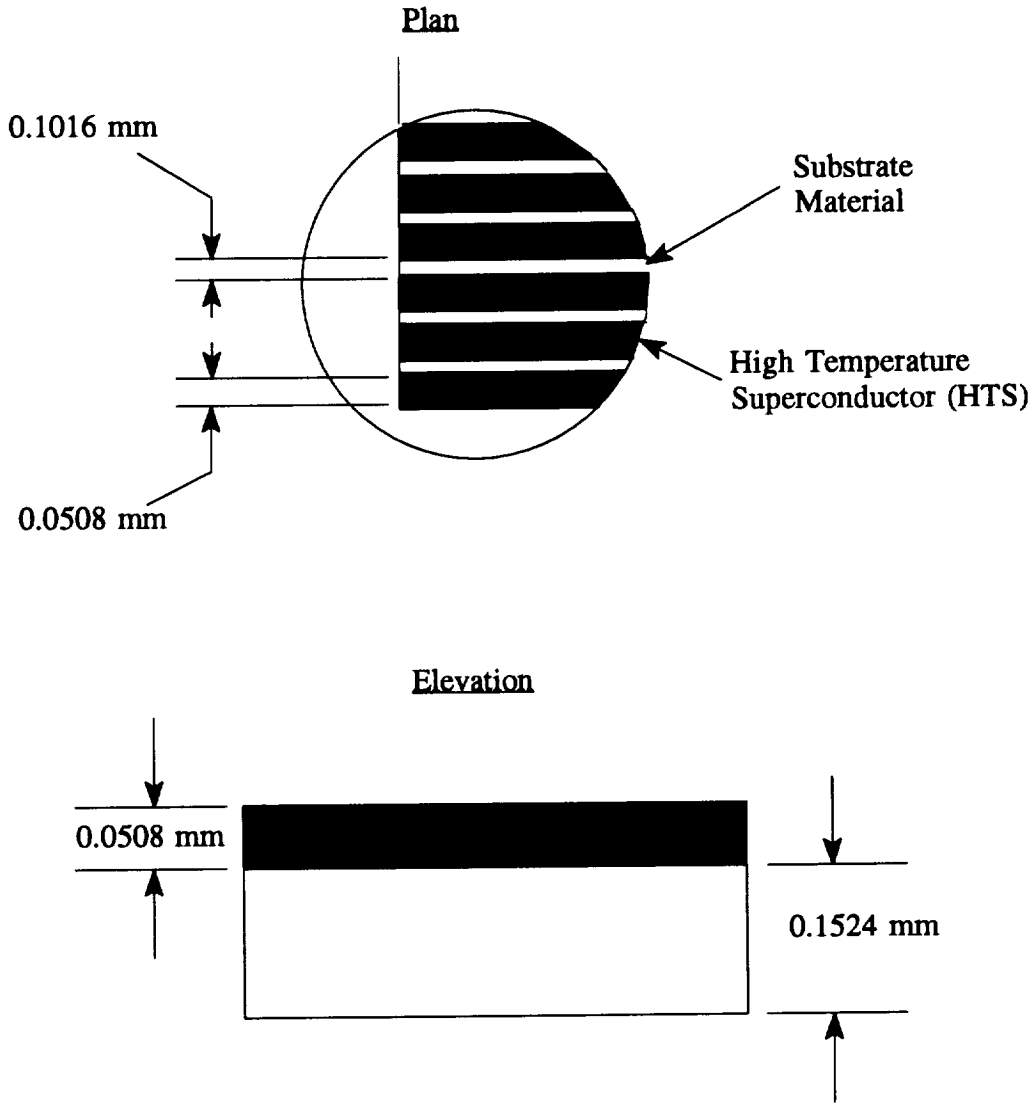

Figure 3.6. Detail A of HTS Leads on Substrate
(Thermal Bridge)

CHAPTER 4

Mathematical Model Analysis

The mathematical models, using programs PATRAN (1990) and SINDA (1985), were constructed to analyze the thermal loads by the electrical leads on the cryogenic system and the temperature distributions along the thermal bridges. The analysis evaluated the effects of two variables: the length of the thermal bridge and the increased or decreased heat flux at the warm end of the electrical leads. All cases include the results which compare the differences of the temperature distributions and the thermal loads on the cryogen between the manganin and the different HTS materials. The following paragraphs summarize the methods used to perform the analysis. Procedures for using the software PATRAN and SINDA are provided in Appendix D.

4.1 Analysis Methodology

The mathematical analysis involves the construction of the thermal bridges in PATRAN and SINDA with the correct boundary conditions that accurately represent the thermal conditions of the thermal bridges (electrical instrumentation) in a sensor satellite. The boundary conditions involve providing a temperature at one end of the thermal bridge and a constant heat flux at the other end. A schematic of the boundary conditions on a HTS thermal bridge is provided as Figure 4.1. The temperature boundary condition, 4 K, represents the cold end of the cryogenic infrared detector. The constant heat flux

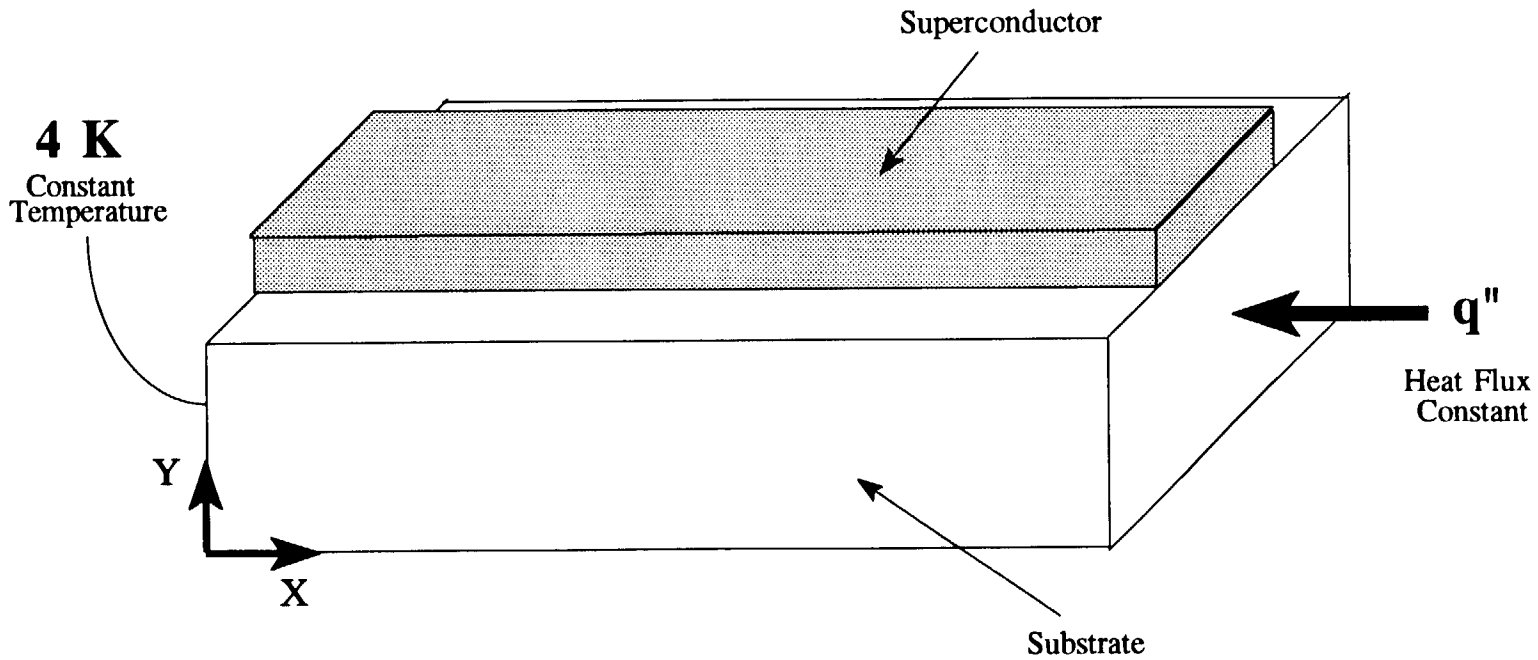

Figure 4.1. Geometric Modeling of the HTS Thermal Bridges

is provided to maintain the heat flux end of the thermal bridge at approximately 80 K to represent the data acquisition and storage systems in a sensor satellite. Using these boundary conditions, the analysis of the temperatures along the x- and y-axis of the thermal bridges is performed. First, the constant heat fluxes were calculated using a one-dimensional parallel flow assumption even though the heat transfer through the thermal bridges is two-dimensional between the HTS leads and the substrate. Then the temperature distribution was calculated with SINDA at the interface of the superconductor and substrate material using a network representation consisting of a series of combinations of the resistances of the substrate and the superconductor materials in parallel configuration as shown in Figure 4.2. This is how SINDA represents two parallel paths in intimate thermal content. Since the heat fluxes were calculated based on the assumption of a one-dimensional parallel flow, the temperature at the location of the applied heat flux may not always be equal to exactly 80 K. In this case, the heat flux was adjusted, i.e. increased or decreased accordingly, until a temperature of 80 K was obtained.

4.2 Heat Flux Calculation

In order to determine the heat flux for the boundary condition of the thermal bridges, the one-dimensional conduction equation

$$q'' = K(T)\frac{dT}{dy}, \tag{4}$$

where $K(T)$ is the thermal conductivity, q'' is the heat flux, T is the temperature, and y is

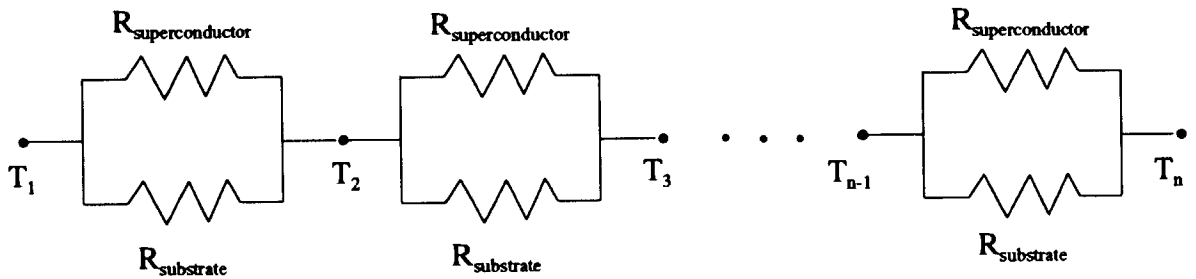

Figure 4.2. Interface Network Model

the distance along the thermal bridges, was used. This equation is solved by separation of variables and integration from 4 K to 80 K while holding q'' constant, that is

$$q'' \int_0^L dy = \int_{4K}^{80K} K(T)dT. \tag{5}$$

Since K is a function of the temperature, integration of the thermal conductivities were determined using the experimental data. Graphs of these experimental data for the thermal conductivities are shown in Figures 4.3 through 4.10. Numerical integration of the thermal conductivities over the temperatures from 4 K to 80 K is performed using a FORTRAN program QFLUX.FOR. Details of this program are included as Appendix A in the thesis. Other thermal conductivity data required for the heat flux calculations are the thermal conductivities of Kapton insulation, which is 0.16 W/m-K (Minco, 1993), and stycast, which is 1.00416 W/m-K (Emerson and Cuming, 1994). The Kapton material is used to insulate the manganin wires from the surrounding and stycast is used to adhere the thermal bridge to the copper block at the cold end in the experimental design. The resulting heat fluxes, calculated by the Fortran program QFLUX.FOR for the different types of materials, are tabulated in Table 4.1.

The heat fluxes for the combination of superconductors and substrate materials were then calculated using the heat fluxes for each component (Table 4.1). Using a parallel flow configuration for the heat transfer through the HTS materials, the heat flux at the warm end can be calculated by first determining the total heat transfer due to the different materials and then dividing the total sum by the total cross-sectional area. For example, consider the $YBa_2Cu_3O_{7-x}$ (YBCO)/Yttrium-Stabilized Zirconia (YSZ) thermal bridge. The YBCO heat flux is multiplied by the total cross-sectional area of the

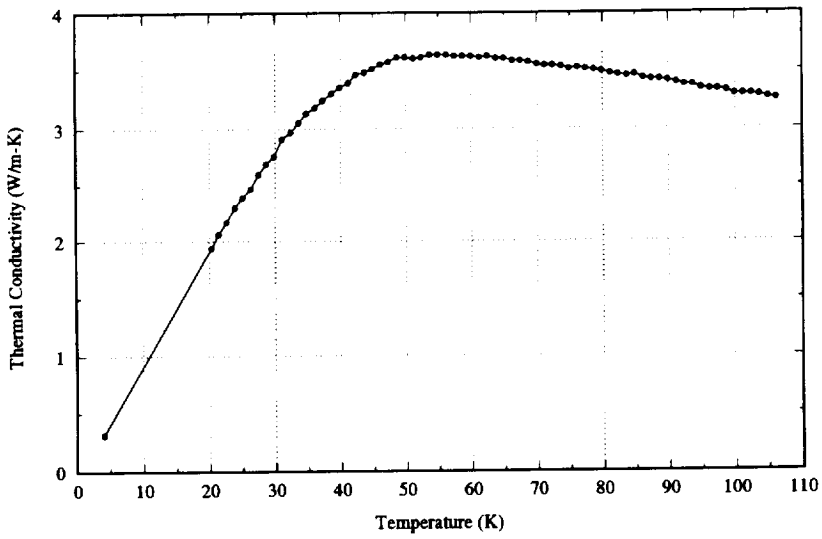

Figure 4.3. Thermal Conductivity of $YBa_2Cu_3O_{7-x}$
(Christopher Newport University, 1993)

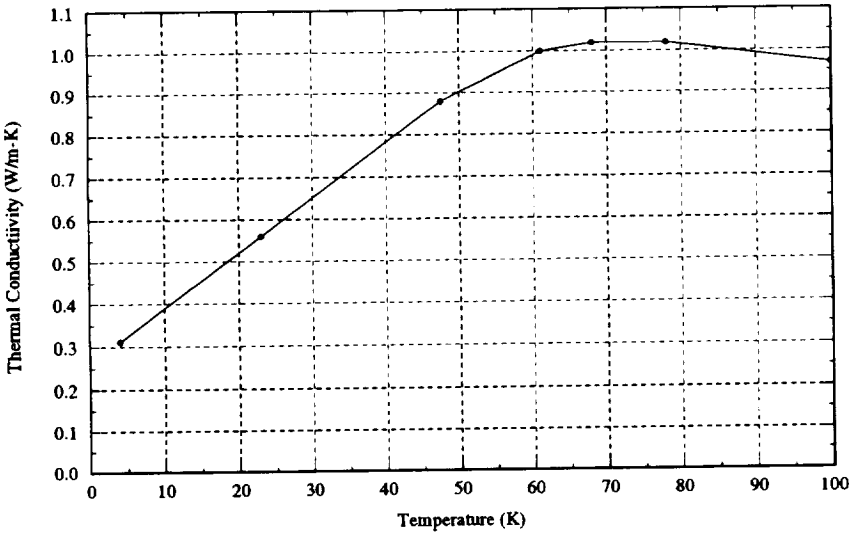

Figure 4.4. Thermal Conductivity of $BiSrCaCu_2O_x$
(Peacor and Uher, 1989)

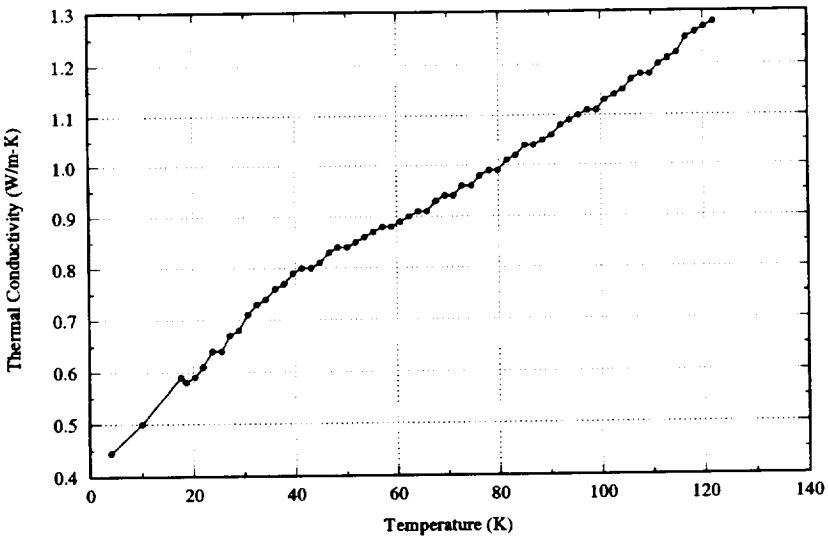

Figure 4.5. Thermal Conductivity of Yttrium-Stabilized Zirconia (Christopher Newport University, 1993)

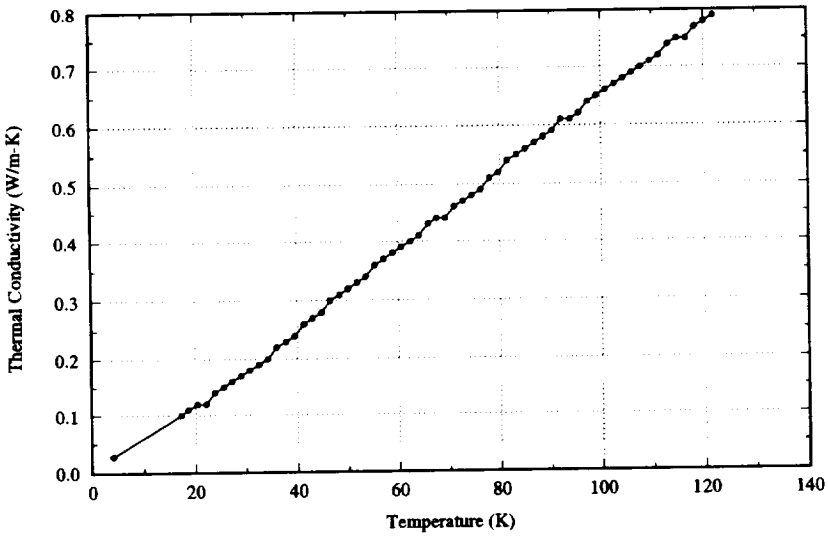

Figure 4.6. Thermal Conductivity of Fused Silica (Christopher Newport University, 1993)

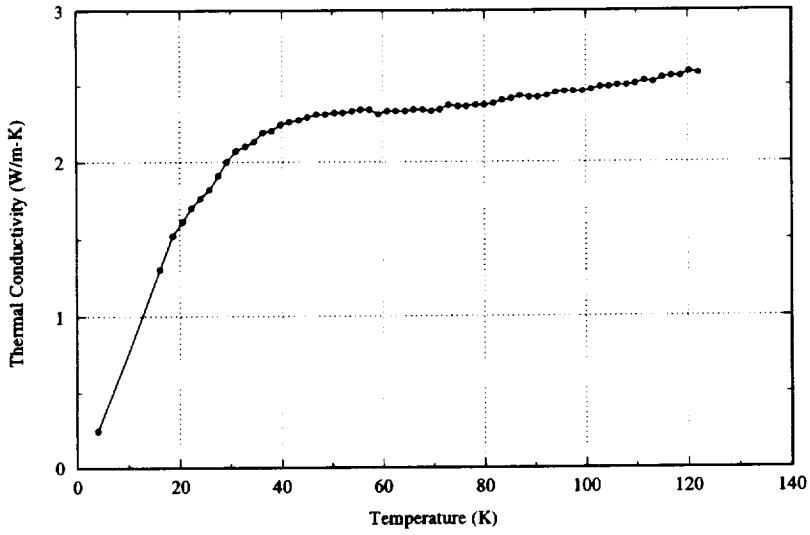

Figure 4.7. Thermal Conductivity of Zirconia
(Christopher Newport University, 1993)

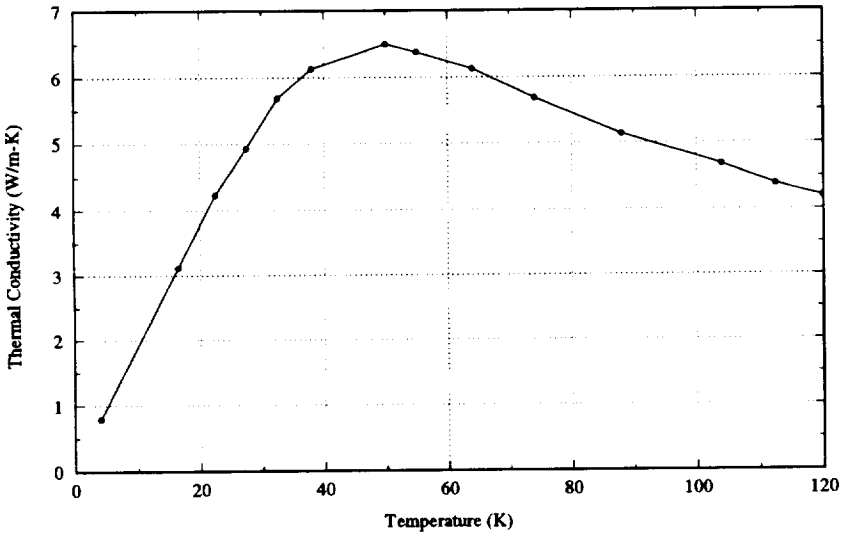

Figure 4.8. Thermal Conductivity of Green (211) Phase
(Christopher Newport University, 1993)

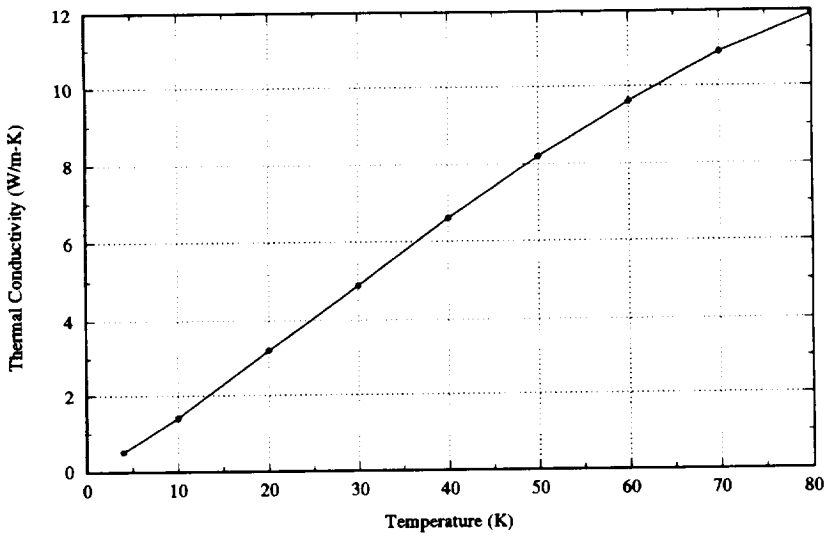

Figure 4.9. Thermal Conductivity of Manganin
(Caton et al, 1992)

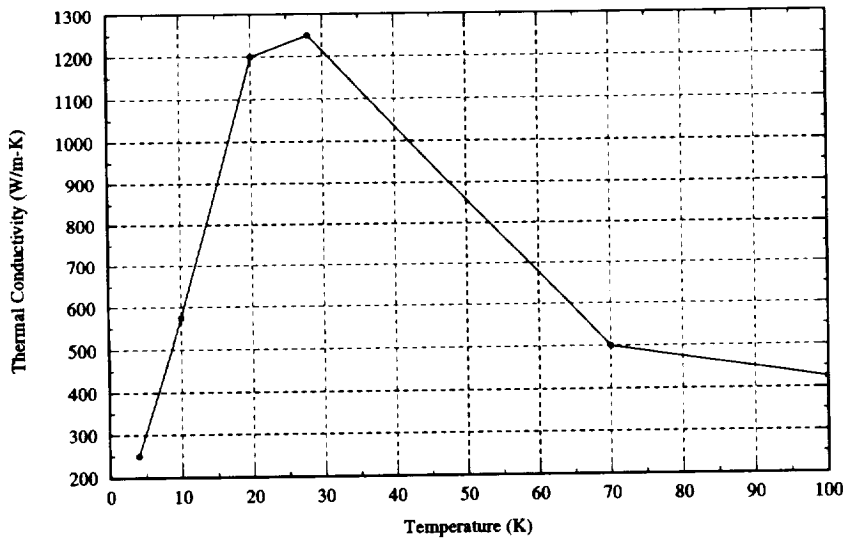

Figure 4.10. Thermal Conductivity of Copper
(APD Cryogenics Inc, 1993)

Table 4.1. Boundary Condition Heat Flux of the Thermal Bridges (152.4 mm)

Materials	Heat Flux (W/m^2) (from QFLUX.FOR)	Heat Flux (W/m^2) (from Curve-Fitting)	Percentage Difference (%)
$YBa_2Cu_3O_{7-x}$	1411.47	1404.94	0.46
$BiSrCaCu_2O_x$	380.05	378.52	0.40
Yttrium-Stabilized Zirconia	380.1	378.78	0.35
Fused Silica (SiO_2)	132.02	131.97	0.04
Zirconia	968.57	972.36	0.39
Manganin	3321.5	3323.84	0.07
Green (211) Phase	2526.98	2529.70	0.11

superconductor leads, 0.1548 mm^2, to obtain the total heat transfer through the leads. The YSZ heat flux is multiplied by the total cross-sectional area of the substrate, 1.3935 mm^2, to determine the total heat transfer through the substrate. Then the heat transfer by the superconductor leads and the substrate are added together to obtain the total heat transfer for this thermal bridge type. Finally, this total value is divided by the total area, 1.548 mm^2, to obtain the heat flux of the YBCO/YSZ thermal bridge. The same method is applied in calculating the heat fluxes of the other superconductor/substrate thermal bridges. These results are tabulated in Table 4.2.

The different cases considered the effect of the lengths (152.4 mm and 101.6 mm)

Table 4.2. Boundary Condition Heat Flux of the Thermal Bridges (152.4 mm) for Different Combinations of HTS Materials and Substrates

Superconductor/Substrate Combination Thermal Bridges	**Heat Flux at the Warm End (W/m^2)**
YBCO/YSZ	483.237
BSCCO/YSZ	380.095
YBCO/Fused Silica*	260.383
BSCCO/Fused Silica*	157.302
YBCO/Green	2415.429
Manganin	3321.5

* indicates the heat fluxes obtained by the program SINDA

and the heat fluxes (1.5 times or 0.5 times the original heat flux used for the 152.4 mm case) on the thermal bridge models. Therefore, the heat fluxes for the various cases are required for performing the mathematical analysis. Since Table 4.2 contains the heat fluxes for 152.4 mm, the heat fluxes for 101.6 mm were calculated by multiplying the given heat flux by the ratios of the lengths. The different values of heat flux of the thermal bridges were obtained by multiplying by 1.5 or 0.5, respectively, to achieve 50 percent higher or 50 percent lower heat fluxes at the boundary condition. The heat fluxes for the superconductors with the fused silica substrates were calculated using the software SINDA. The calculated values did not originally correspond accurately to a temperature of 80 K at the heat flux end of the thermal bridges. Therefore, the heat flux value at this end of the thermal bridge was modified, i.e. increased or decreased, in the SINDA input file until this end temperature reached approximately 80 K.

4.2.1 Verification of the Heat Flux at the Warm End

The thermal conductivity plots (Figures 4.3 to 4.10) for the material were curve-fitted to obtain the equations, provided in Appendix B, of the thermal conductivities, K(T). Then the equations were integrated with respect to temperature and multiplied by the length of the thermal bridge to determine the heat fluxes, tabulated in Table 4.1. Also in Table 4.1, these results are compared to the heat fluxes determined by the FORTRAN program in QFLUX.FOR. The comparison indicates that the heat fluxes calculated from the two different methods correlate to each other within 0.5 percent and therefore, verifies the program QFLUX.FOR used to calculate the heat fluxes using the experimental data.

4.3 Geometric Modeling of the Thermal Bridges

PATRAN is used as the pre- and post-processing software to construct and mesh (divide) the geometric model of the thermal bridge into nodes and elements. SINDA, a finite difference program, is used to obtain the temperature distributions along the thermal bridges and the heat transfer into and out of the models. Interface software is implemented between PATRAN and SINDA to shuttle the data back and forth between these two programs.

The three types of geometric model in the analysis are the manganin wires, the superconductor leads printed on a substrate, and the superconductor leads with buffer layers printed on a substrate. The manganin wires were modeled as a single wire due to the assumed one-dimensionality of the problem. In addition, the resistance self-heating through the manganin wires was neglected in this analysis to simplify the heat transfer

analysis through the manganin leads. Since the HTS materials do not have electrical resistance at cryogenic conditions, the comparison of the heat transfer through the manganin and the HTS materials will be conservative.

The two types of the HTS thermal bridges were modeled similarly to each other except for the buffer layer, which is the material placed between the superconductor and the lead. Since radiation and convection were assumed to be negligible, i.e. no external heat transfer, the problem was simplified by lumping the individual leads of the HTS materials as a single lead on the substrate. As part of simplifying the modeling process further, one-half of the HTS thermal bridges were modeled by using an insulated boundary condition at the plane of symmetry in addition to lumping the HTS leads as a single lead. The initial intention was to model the individual HTS leads on a substrate in order to be able to incorporate the radiation into the experimental design in the future. However, even running this symmetrical model proved to be an inefficient process. In fact, a first run of the symmetric model for the YBCO/YSZ thermal bridge of 152.4 mm in length indicated that the temperatures did not converge after 50 hours of running time. The expected temperature at the warm end of the thermal bridge is approximately 80 K, but the temperature only reached 78.5 K. In order for the model to converge within a reasonable running time, the number of iterations needed to be reduced. The number of iterations depends on the nodes and elements of the finite difference model of the thermal bridges. Therefore, the running time depends on the number of nodes and elements. Hence, only one-half of the thermal bridge was modeled assuming a single-lead printed on a substrate to minimize the number of nodes and elements.

In order to validate this simplification, the symmetrical model (with individual leads) of a shorter YBCO/YSZ thermal bridge (101.6 mm in length) was first modeled with PATRAN and analyzed by the SINDA program. Then, a simplified model (with lumped leads) of the same material was constructed and analyzed. The temperature distributions for the symmetrical model and the simplified model of the YBCO/YSZ thermal bridge (101.6 mm) are provided as Figure 4.11. The two curves on this figure indicate that the temperature distributions correlate within 0.6 percent which is an acceptable allowance for using this simplified model in place of the original, symmetrical model of the HTS thermal bridge.

4.4 Finite Difference Method

The software PATRAN was used to build the geometric model of the thermal bridges, and then SINDA was used to divide the geometric shapes into elements and nodes for the finite difference method. These results from PATRAN are referred to as the node and conductor data and are inputs to the SINDA input file. The SINDA input file was created to solve a steady-state problem. The results from SINDA analysis were the temperature distributions and the heat transferred in and out of the thermal bridges. Details of running the programs PATRAN and SINDA are provided in Appendix C and D, respectively.

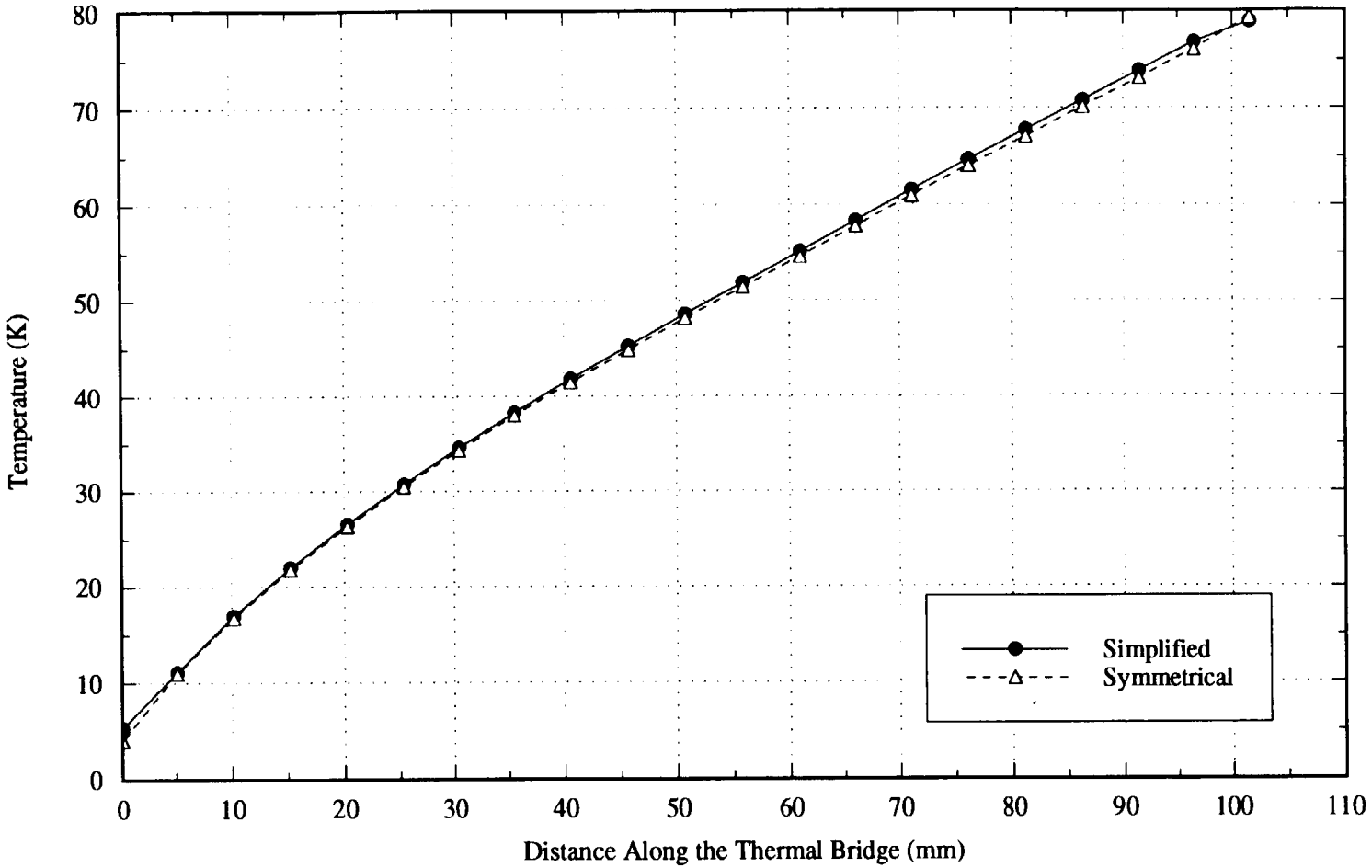

Figure 4.11. Comparison of 101.6 mm Thermal Bridge Models (YBCO/YSZ Materials)

CHAPTER 5

Results and Discussion

The following subsections contain the comparison of the results between the HTS materials and the manganin wires. In addition, the temperature distributions and the heat transfer in and out of the thermal bridges for the two case studies comparing the effects of the lengths and the heat fluxes on the different types of the thermal bridges are given. The temperature distributions are not intended to determine the heat load on the cryogen. Their main purpose is to provide temperature gradients to be used in the future thermal conductivity measurements. In addition, the temperature distributions for the manganin wires do not take into consideration the electrical self-heating and, therefore, the results for the manganin are conservative estimates.

5.1 Effect of the Thermal Bridge Length

Two different lengths of the thermal bridges were analyzed to study the effect of the length on the temperature distribution and the heat load on the cryogen. The overall behavior of the temperature distribution for each type of material did not change when the lengths of the thermal bridges were changed. In fact, the temperature distributions for each model stayed relatively similar, as shown in Figures 5.1 and 5.2 for the 152.4 mm and 101.6 mm lengths, respectively. However, the temperature distribution for manganin is higher in comparison to the distributions of the HTS materials. As

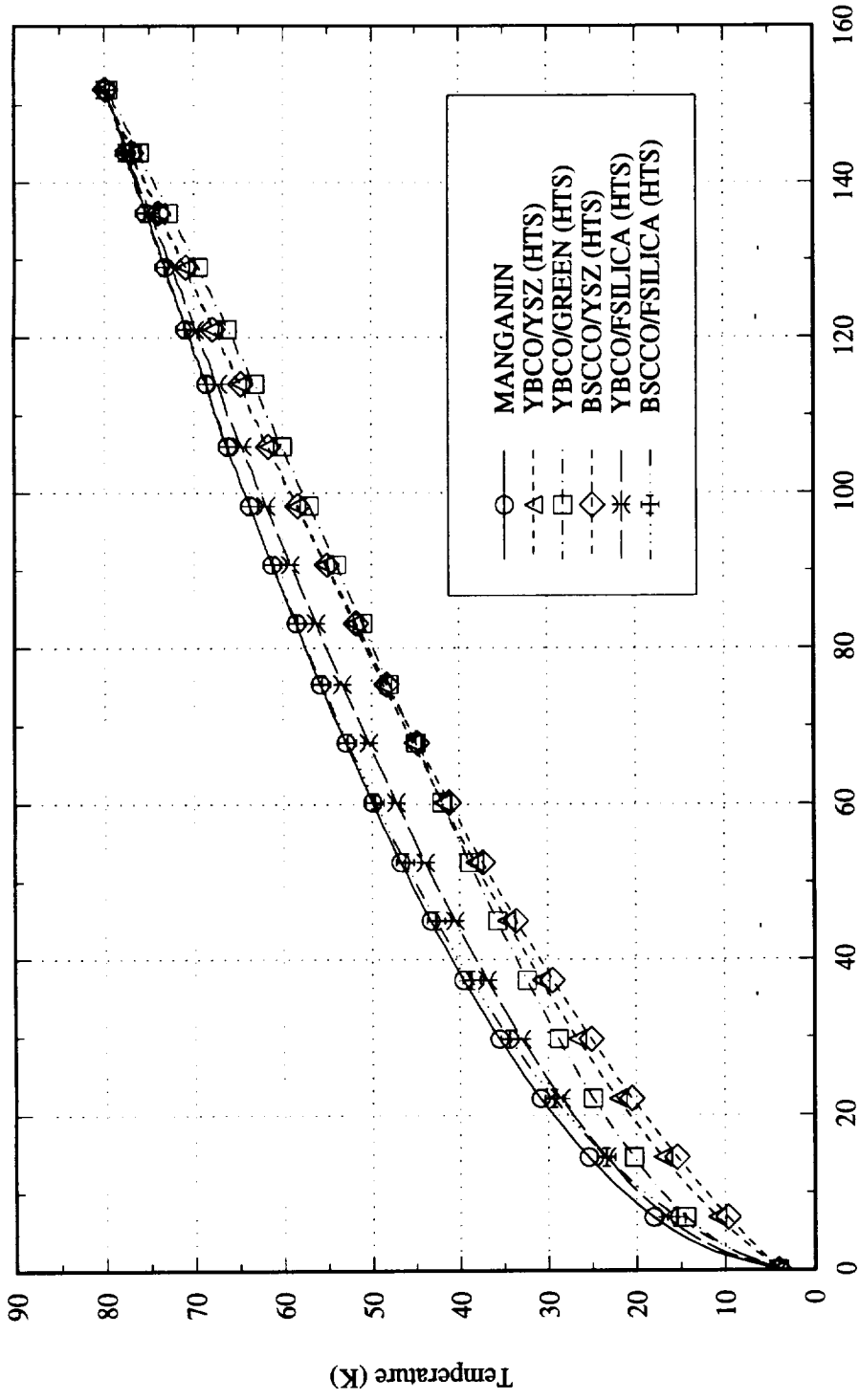

Figure 5.1. Temperature Distributions of Thermal Bridges (152.4 mm Long)

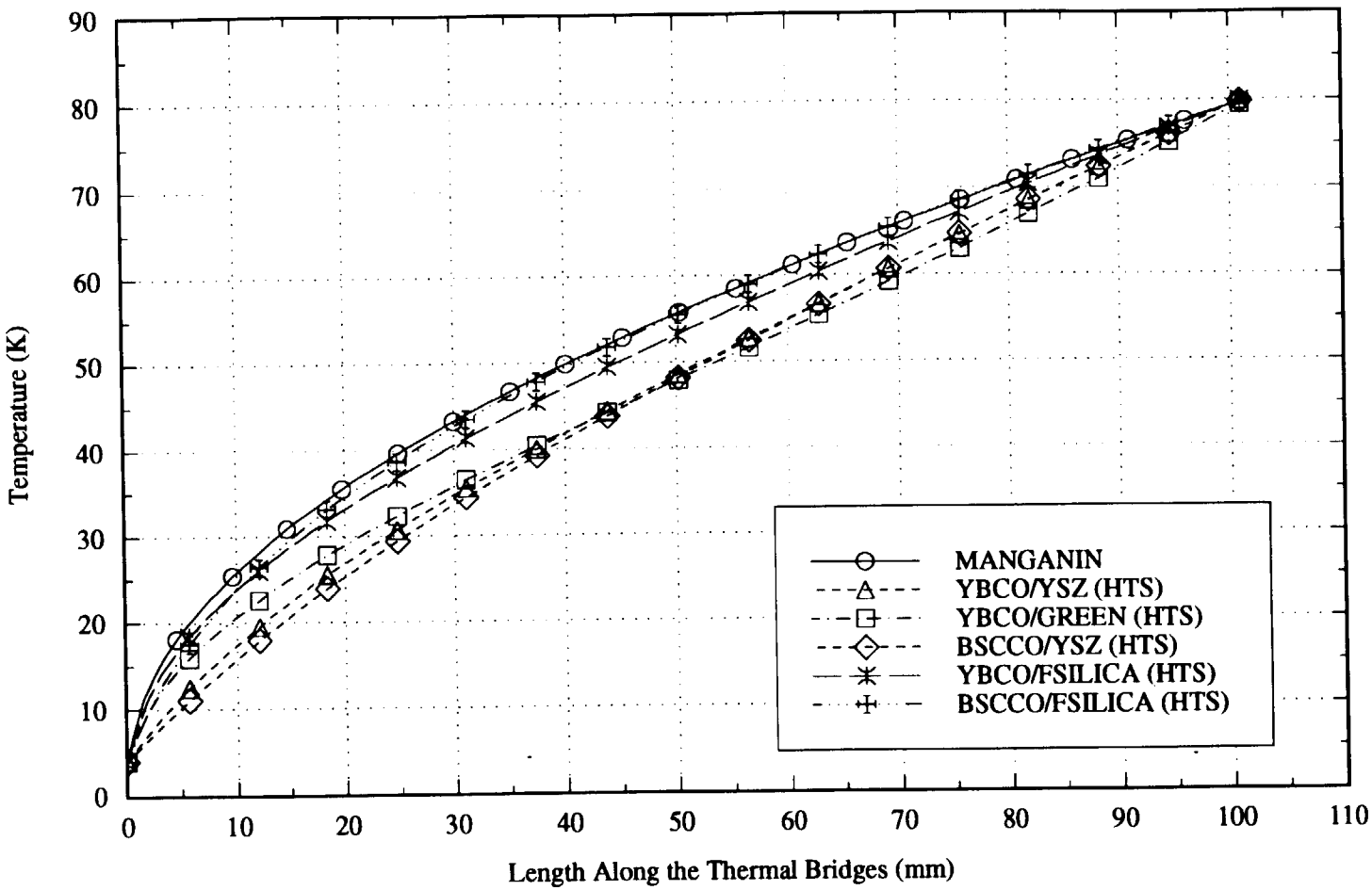

Figure 5.2. Temperature Distributions of Thermal Bridges (101.6 mm)

mentioned earlier, the temperature distributions of manganin do not include Joulean heating. However, this effect will be included in future work pertaining to this research.

The temperature distributions do not aid in determining which materials are the best candidates for minimizing the heat transfer to the detector. The best candidates are the temperature gradient and the thermal conductivity of the materials since the heat transfer due to conduction follows Fourier Law. Since the temperature distributions do not clearly show which materials have the larger temperature gradients, there is no obvious indication that an HTS thermal bridge has lower heat flow than the manganin leads.

However, an interesting result may be seen from Figures 5.1 and 5.2. For the materials $YBa_2Cu_3O_{7-x}$ (YBCO) lines on yttria-stabilized zirconia (YSZ, 10wt%, cubic) and $BiSrCaCu_2O_x$ (BSCCO) lines on YSZ, the temperature distributions along the length of the thermal bridges have a strong correlation. According to Fourier's law, if the materials have similar temperature gradients with a constant heat flux, the overall resistance should be the same. Since these two materials have similar temperature gradients, their resistance should be closely related. The overall resistance for the HTS thermal bridges consist of the thermal conductivities of the superconductor and the substrate. In order for the resistance to be similar between the YBCO/YSZ and the BSCCO/YSZ thermal bridges, the substrate must be the dominant factor in the determination of the heat flow through the thermal bridges.

5.2 Effect of the Heat Flux

The effect of increasing and decreasing the individual heat flux for each thermal bridge is different. The different boundary conditions were implemented in the analysis by changing the heat flux values in the SINDA input file, Appendix D. Figure 5.3 shows the effect of higher heat flux and it shows that the HTS materials are no longer desirable at a temperature greater than 80 K, because beyond this temperature the slope of the temperature distributions for the HTS materials are steeper than that of manganin. The steeper slope indicates higher temperature gradients which can possibly translate to a higher heat transfer. This observation is not a clear indication that the heat transfer through the thermal bridges are greater than manganin since the heat transfer is both a function of temperature gradients and thermal conductivities.

However, the results of Figure 5.3 consider the electrical ramifications of using HTS materials. There is "a rule of thumb" that the superconductors can be used in applications which operate at or below 3/4 of their critical temperature since, at this point, the superconductors have reached almost 1/4 of their critical current density. In order to use the superconductors in the sensor satellite, they must be operated at temperatures at or below 80 K since their critical temperatures are 95 K for the YBCO and 100 K for BSCCO. Therefore, these superconductors are not electrically sufficient to be used in applications beyond 80 K.

The temperature distributions for the lower heat flux case are plotted in Figure 5.4. These plots indicate similar behavior to the ones encountered for the 152.4 mm case in Figure 5.1, with the manganin thermal bridge displaying a higher temperature distribution

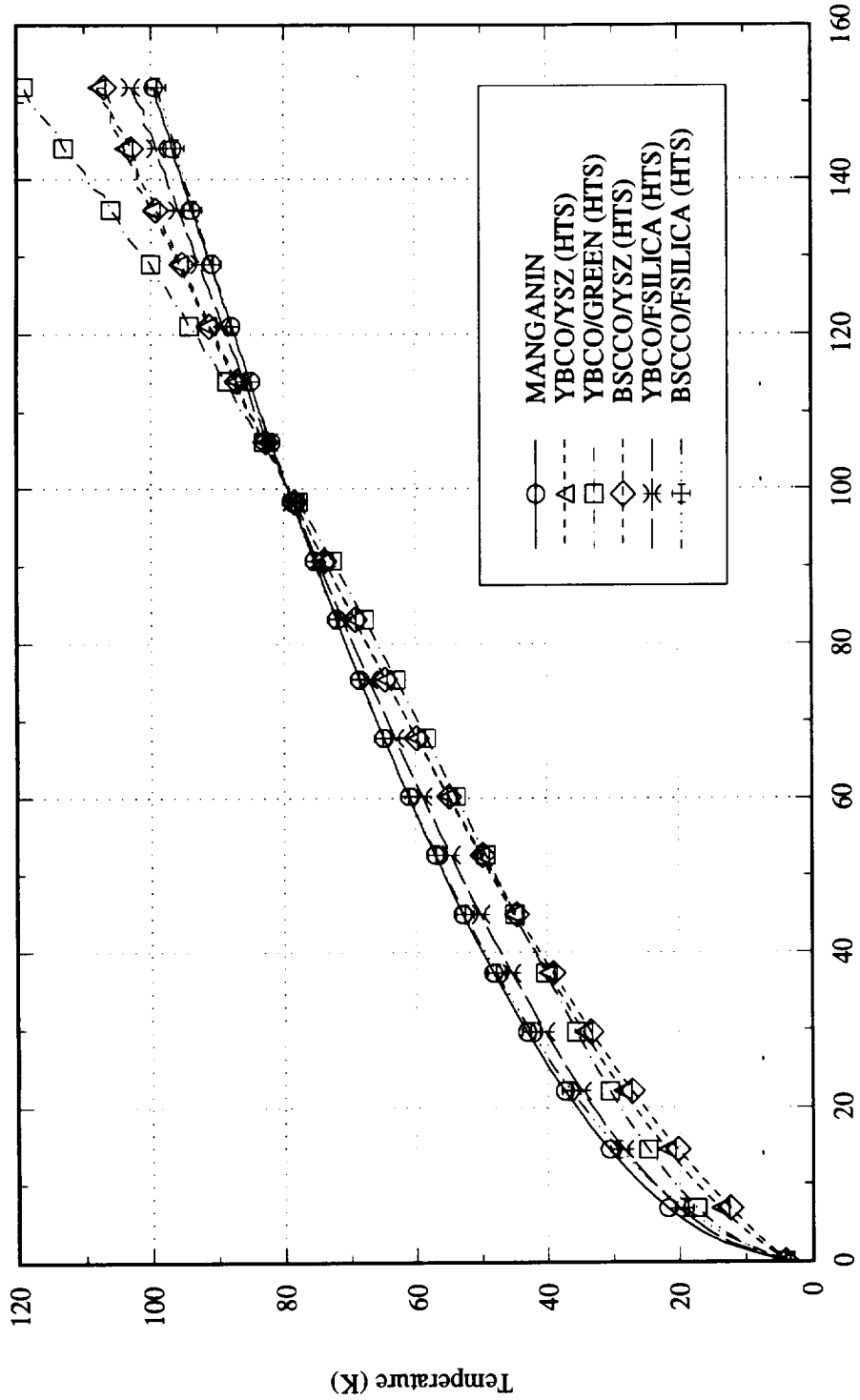

Figure 5.3. Temperature Distributions of Thermal Bridges (152.4 mm Long) with 50% Higher Heat Flux

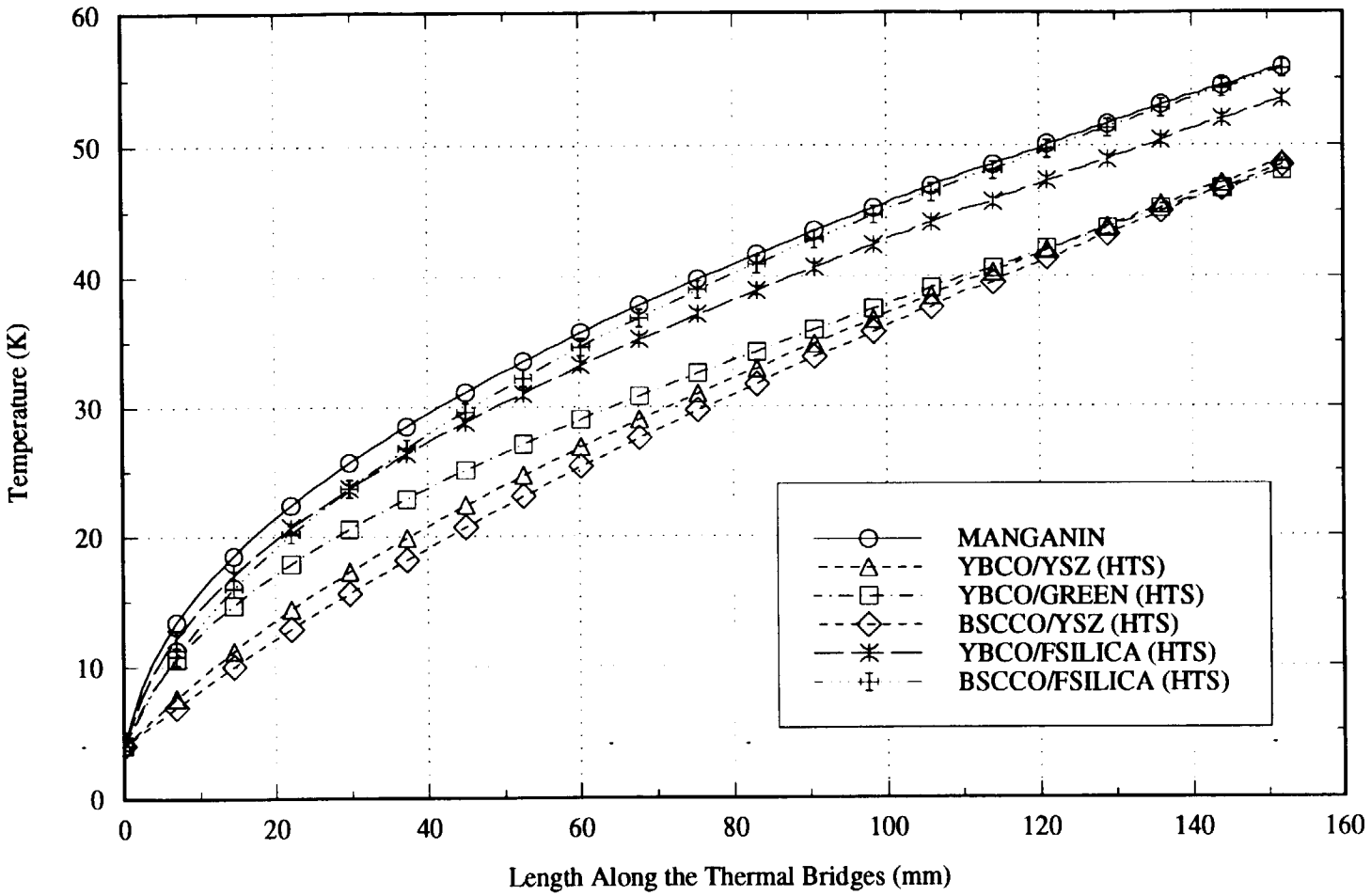

Figure 5.4. Temperature Distributions of Thermal Bridges (152.4 mm Long) with 50% Lower Heat Flux

than the HTS thermal bridges. However, the results for the HTS thermal bridges are relatively similar to each another in comparison.

5.3 Thermal Load on the Cryogen

The heat loads using the different thermal bridge materials are tabulated in Table 5.1. In first considering the effect of the length for each material, the results indicate that longer thermal bridges have lower heat loads than the shorter ones, as expected. Considering the effect of heat flux, the heat loads associated with larger heat fluxes are larger than those associated with the lower heat fluxes, also as one would expect. Finally, the HTS materials display a lower heat load when compared to the manganin wires. The results obtained are the heat flux calculated earlier in Table 4.1 multiplied by the cross-sectional area.

Earlier investigations by NASA (Wise et al., 1992) have indicated that the heat load placed on the cryogen by the manganin wires is at least 20 percent of the total heat load on the cryogen. First, the heat load on the cryogen due to 152.4 mm long manganin was assumed to be 20 percent. Then, the heat load by the other materials were calculated in comparison to the manganin (152.4 mm long) and tabulated as Table 5.2. The results indicate a minimum of almost 5 percent heat load on the cryogen due to the HTS thermal bridges (specifically the $BiSrCaCu_2O_x$ on Fused Silica substrate) which is almost a 15 percent reduction in the heat load being currently placed on the cryogen by the manganin wires. In terms of the satellite mission lifetime, a 15 percent savings means over 9-month extension on a satellite with 5-year mission.

Table 5.1. Heat Load on the Cryogen Due to Different Types of Thermal Bridges

Cases	Parameters	Heat Load by Different Types of Thermal Bridge Materials (W)					
		Manganin (W)	YBCO/YSZ (W)	BSCCO/ YSZ (W)	YBCO/ GREEN (W)	YBCO/ FSILICA (W)	BSCCO/ FSILICA (W)
a	**152.4 mm Long**	.001	.000748	.000589	.00374	.000403	.000244
b	**101.6 mm Long**	.0015	.00112	.000883	.00561	.000605	.000366
c	**Higher Heat Flux (50%)**	.0015	.00112	.000883	.00561	.000605	.000366
d	**Lower Heat Flux (50%)**	.0005	.000374	.000294	.00187	.000202	.000122

Table 5.2. Percentage of Heat Load on the Cryogen by the Thermal Bridges in Comparison with the Manganin Wires of 152.4 mm Length

Cases	Parameters	Total Heat Load on the Cryogen by the Thermal Bridges (%)*					
		Manganin (%)	YBCO/ YSZ (%)	BSCCO/ YSZ (%)	YBCO/ GREEN (%)	YBCO/ FSILICA (%)	BSCCO/ FSILICA (%)
a	**152.4 mm Long**	20.0	14.9	11.7	74.7	8.1	4.9
b	**1016 mm Long**	30.1	22.5	17.7	112.6	12.1	7.3
c	**Higher Heat Flux (50%)**	30.1	22.5	17.7	112.4	12.1	7.3
d	**Lower Heat Flux (50%)**	10.0	7.5	5.9	37.3	4.0	2.4

* in comparison with manganin leads of case a.

For the case of 152.4 mm length, the BSCCO/FSILICA combination has the smallest percentage of the heat load (4.9 percent) on the cryogen and the YBCO/GREEN has the largest heat load (74.7 percent) compared to the other materials. The heat load for the next case of 101.6 mm length, which shows smaller heat load (7.3 percent) for BSCCO/FSILICA and larger heat load (112.6 percent) for YBCO/GREEN, are greater than the results for the 152.4 mm long case, but the order of smallest-to-largest heat load on the cryogen among the materials is identical to the one for the 152.4 mm case.

The next consideration is the effect of the heat flux on the thermal bridges. The order of the BSCCO/FSILICA combination having the smallest heat load (7.3 percent) and the YBCO/GREEN thermal bridge having the largest heat load (112.4 percent) are repeated for the cases of the higher and the lower heat flux of the thermal bridges. The higher heat flux indicates higher heat load and the lower heat flux indicates lower heat load in comparison to the first case study (case a in Table 5.2).

One of the objectives of this research was to compare quantitatively the performance of the HTS materials with the manganin wires, and one method to accomplish this objective is to accurately model the thermal conditions of the sensor satellite within the experimental design. Since the temperature at the warm end of the thermal bridges needs to be at approximately 80 K, the case study of the heat flux is not as applicable as the effect of the length. However, the allowable lengths for the thermal bridges are limited to the range from 101.6 mm to 152.4 mm.

Since the goal of the research is to minimize the heat load on the cryogen, i.e. increase the thermal savings, the results for the 152.4 mm long bridge (case a) are more desirable for further investigation. Amongst the thermal bridges for this particular case, the lowest heat load of 5.2 percent can be obtained by using the BSCCO/FSILICA thermal bridge. Therefore, assuming that the total heat load by current manganin leads are 20 percent, the total heat load by the electrical leads can be reduced by 15.1 percent. This percentage is the amount of the cryogen which can be saved in cooling the detector. Hence, the 15.1 percent cryogen savings translates to over a 9-month extension on a five-year mission. The extension on the life of a 5-year mission by replacing the currently used manganin wires are summarized as Table 5.3. The minus sign in Table 5.3 indicates that the life of the mission satellite is reduced by the indicated amount if this particular type of thermal bridge is used. The maximum life extension of 9.1 months can be achieved by using the BSCCO/FSILICA thermal bridge material in place of the manganin wires.

The material with the maximum life extension correlates to the material with the lowest heat load, as mentioned earlier. The next smallest heat load of 8.1 percent can be obtained by YBCO/FSILICA thermal bridge which is a 3.2 percent higher heat load than BSCCO/FSILICA model. From Figures 4.2 and 4.3, the thermal conductivities of the superconductors, YBCO and BSCCO are seen to be different. In fact, YBCO has almost three times the thermal conductivity of the BSCCO superconductor. Since the heat transfer through the thermal bridges are functions of the thermal conductivity and the temperature gradients, the results should indicate that YBCO has a significantly larger

Table 5.3. Extended Life on a 5-Year Mission Satellite

Cases	Parameters	Extended Life Beyond Five Years (months)					
		Manganin	YBCO/ YSZ	BSCCO/ YSZ	YBCO/ GREEN	YBCO/ FSILICA	BSCCO/ FSILICA
a	**152.4 mm Long**	0.0	+3.0	+4.95	-32.8	+7.2	+9.1
b	**1016 mm Long**	-6.1	-1.5	+1.4	-55.4	+4.7	+7.6
c	**Higher Heat Flux (50%)**	-6.1	-1.5	+1.4	-55.4	+4.7	+7.6
d	**Lower Heat Flux (50%)**	+6.0	+7.5	+8.5	-10.4	+9.6	+10.5

heat load than the BSCCO because of its larger thermal conductivity. However, that is not the case as mentioned earlier since the thermal savings by these two superconductors differ by 3.2 percent. Since the heat transfer through the thermal bridges takes into effect both the thermal conductivities of the superconductor and substrate material and since the substrate material for these combinations of thermal bridges is the same, the observation is that the substrate material seems to be the driving force in determining the thermal savings. As a confirmation, compare the thermal conductivities of the Green phase with the YSZ and Fused Silica substrates, as shown in Figure 5.5. These plots of Figure 5.5 indicate that the thermal conductivities ranging from largest to smallest places in order the substrate GREEN first followed by YSZ and then by fused silica. The results from Table 5.1 follow the same scheme for YBCO printed on the mentioned substrates, GREEN, YSZ, and fused silica. The YBCO/fused silica has the lowest heat load (highest thermal savings) in comparison to the YBCO/YSZ and YBCO/GREEN. Therefore, the substrate material indeed has the most effect on the heat transfer through the thermal bridges and hence, the thermal savings.

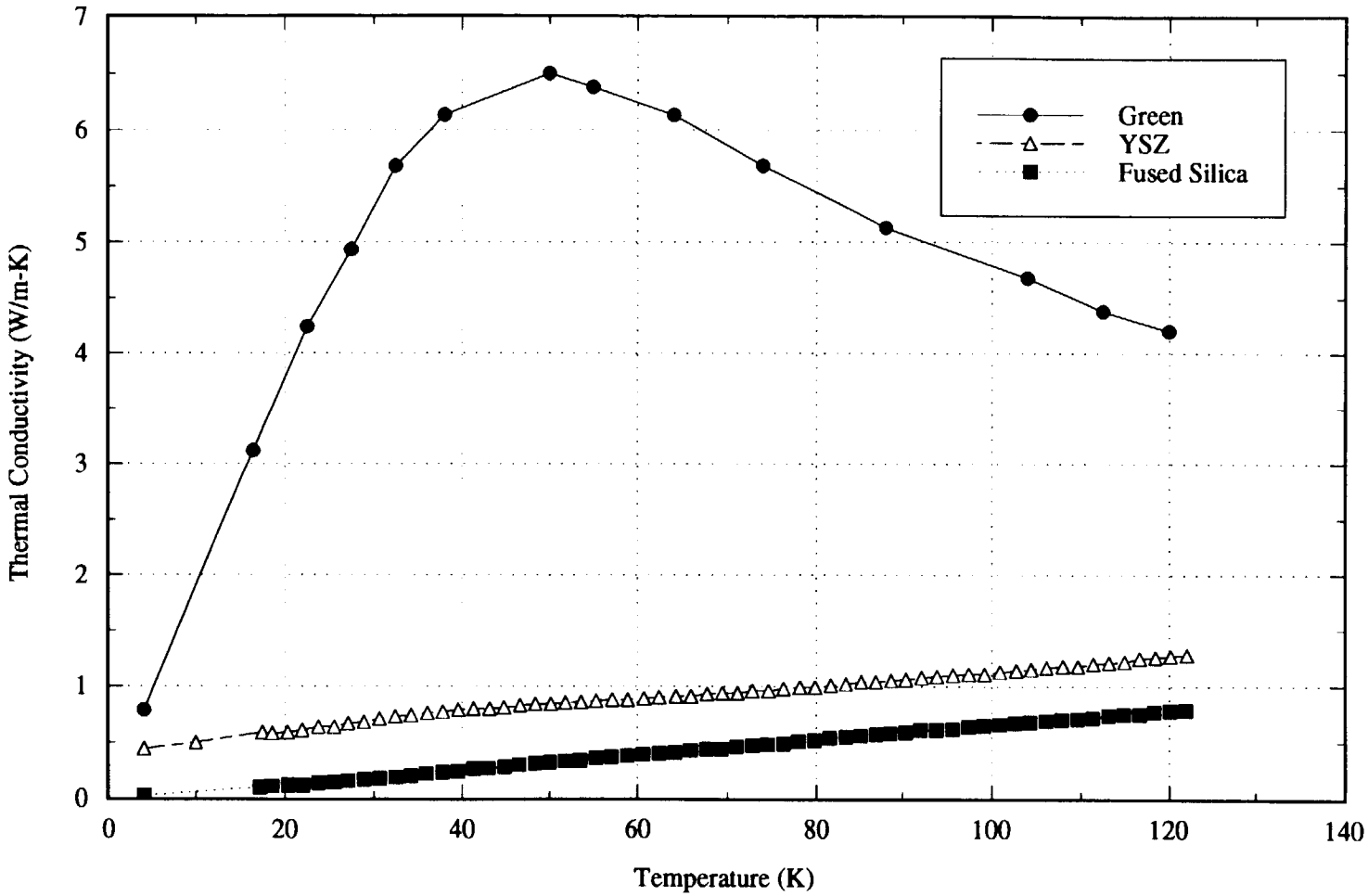

Figure 5.5. Thermal Conductivities of the Substrate Materials

CHAPTER 6

Conclusion

The goal of the research project was to assess the feasibility of replacing the currently used manganin wires with the HTS materials printed on ceramic type substrates as electronic leads in cryogenic infrared sensor satellites. The research included designing an experiment which measures the heat loss through the different materials and the thermal conductivity of the HTS materials in space. As part of the investigation, five combinations of superconductor/substrate thermal bridges were compared to the manganin. These combinations are $YBa_2Cu_3O_{7-x}$ lines on yttria-stabilized zirconia (YSZ, 10wtpercent, cubic); $BiSrCaCu_2O_x$ lines on YSZ; $YBa_2Cu_3O_{7-x}$ lines on fused silica (3000 angstroms buffer layer of zirconia); $BiSrCaCu_2O_x$ lines on fused silica (3000 angstroms buffer layer of zirconia); and $YBa_2Cu_3O_{7-x}$ lines on 211 (Green) Phase. The results, summarized in Table 5.2, indicated that in the worst case there is over 74.7 percent and for the best case there is less than 5 percent heat load by the electrical instrumentation (thermal bridges) on the cryogen if the manganin wires are replaced by the HTS thermal bridges. In fact, four of the five HTS materials showed heat loads less than 15 percent. Considering the currently used manganin wires display heat load of about 20 percent, most of the HTS thermal bridges are potential replacements for the manganin wires as electronic leads in cryogenic infrared sensor satellites.

CHAPTER 7

Recommendations for Future Studies

For the short-term, there are several important analyses which need to be performed before the experiment can be ready for actual spaceflight. First, the support mechanism for the HTS thermal bridges needs to be selected and then qualified structurally for a potential spaceflight. The design of the support system is currently underway. The conduction analysis of the supports need to be incorporated into the current experimental design to accurately model the thermal bridges. In addition, a radiative-conductive mathematical model of the thermal bridges needs to be constructed and added to the thermal analysis of the thermal bridges (electrical instrumentation). Although the radiation effect on the thermal bridges is expected to be negligible in comparison to the conduction, the radiation can be a significant factor when a model is analyzed in the environment of a vacuum with low temperatures.

Considering the results of the mathematical analysis indicating a strong correlation between the substrate material and the heat transfer through the HTS thermal bridges, it is important to select the substrate with lower thermal conductivity in minimizing the heat transfer. In addition, if the dimensions of the substrate can be decreased, the heat transfer through the HTS thermal bridges will also decrease.

Another key feature which needs to be incorporated into the current experimental design is to send electronic signals through the leads. Currently, there is no measurement

which can be made to determine if or when a superconductor lead is destroyed or damaged. Currently, any failure in the leads will render the entire data collected in space invalid because there is no way to determine when the data became corrupted. By sending an electronic signal through the leads and monitoring the signals, the time at which a superconductor leads fail can be determined. If it is determined that the lead cracked after the launch, all data are invalid. If it however was destroyed during the landing, the data collected for the mission is still valid. This means that the acceptable data will not be declared useless in the case of the second scenario. In addition, this feature will offer the method to obtain the effective heat transfer through the manganin wires.

For a long-term, a prototype of the final experimental design will be built for ground testing. The ground tested experiment will be modified accordingly to be ready for a spaceflight mission on the shuttle.

BIBLIOGRAPHY

Allen, N.P., ed. by David Fishlock, 1969, *Guide to Superconductivity*, MacDonald & Co., London, pp. 1 - 16.

Aslam, M., R. E. Soltis, E. M. Logothetis, R. Ager, M. Mikkor, W. Win, J. T. Chen, and L. E. Wenger, 1988, "Rapid Thermal Annealing of YBaCuO Films on Si and SiO_2 Substrates," Applied Physics Letters, 53(2):153-155.

APD Cryogenics Inc., 1993, Allentown, PA, (215) 791-6750.

Baixeras, J., F. H. Teherani, A. Kreisler, A. Straboni and K. Barla, 1990, "Thin Films of YBaCuO for Electronic Applications," SPIE: Physical Concepts of Materials for Novel Optoelectronic Device Applications II (Device Physics and Applications), 1362:117-126.

Bansal, N. P., R. N. Simons, and D. E. Farrell, 1988, "High T_c Screen-printed $YBa_2Cu_3O_{7-x}$ Films: Effect of the Substrate Material," Applied Physics Letters, 53(7):603-605.

Bardeen, J., ed. by M. H. Cohen, 1968, *Superconductivity in Science and Technology*, Chicago: University of Chicago Press, 1-17.

Beck, J.V., and Arnold, K.J., 1977, Parameter Estimation in Engineering and Science, John Wiley and Sons, New York.

Budhani, R.C., Sing-Mo H. Tzeng, H. J. Doerr, and R.F. Bunshah, 1987, "Synthesis of Superconducting Films of the Y-Ba-Cu-O System By a Screen Printing Method," Applied Physics Letters, 51(16):1277-1279.

Castles, S., S. Breon, M. Viens, C. Allen, R. Patschke, K. Stewart, H. Moseley, J. Brasunas, L. Hilliard, C. Richards, and Y. Flom, 1988, *World Congress on Superconductivity: Progress in High Temperature Superconductivity*, World Scientific, New Jersey, 8:155-167.

Caton, R., R. Selim, and A. M. Buoncristiani, 1992, "A Comparison of Superconductor and Manganin Technology for Electronic Links Used in Space Mission Applications," NASA Contractor Report 4477.

Choi, B. I., Z. M. Zhang, M. I. Flik and T. Siegrist, 1992, "Radiative Properties of Y-Ba-Cu-O Films With Variable Oxygen Content," Transactions of the ASME,

114:958-964.

Cima, M. J., J. S. Schneider, S. C. Peterson, and W. Coblenz, 1988, "Reaction of $Ba_2YCu_3O_{6.9}$ Films With Yttria-Stabilized Zirconia Substrates," Applied Physics Letters, 53(8):710-712.

Creel, K. E., and D. J. Nelson, 1994, "A Thermal Analysis Tool for Three-Dimensional Thermal Models of Multilayer Microelectronics," Proceedings of the Virginia Power Electronics Center Seminar, Virginia Tech, Blacksburg, VA, pp. 113-127.

Dernbach, D. and K. H. Ehses, 1990, "Thermal Expansion and Symmetry of $Y_1Ba_2Cu_3O_7$," Journal of the Less-Common Metals, Elsevier Sequoia, The Netherlands, 164 & 165: 146-151.

Ekin, J. W., A. I. Braginski, A. J. Panson, M. A. Janocko, D. W. Capone II, N. J. Zaluzec, B. Flandermeyer, O. F. de Lima, M. Hong, J. Kwo and S. H. Liou, 1987, "Evidence for Weak Link and Anisotropy Limitations on the Transport Critical Current in Bulk Polycrystalline $Y_1Ba_2Cu_3O_x$," Journal of Applied Physics, 62(12):4821-4828.

Emerson and Cuming Co., 1994, Woburn, MA.

Geballe, T. H. and J. K. Hulm, 1988, "Superconductivity - The State That Came in From the Cold," Science, 239:367-375.

Gurvitch, M. and A. T. Fiory, 1987, "Preparation and Substrate Reactions of Superconducting Y-Ba-Cu-O Films," Applied Physics Letters, 51(13):1027-1029.

Hagen, S. J., Z. Z. Wang, and N. P. Ong, 1989, "Anisotropy of the Thermal Conductivity of $Y_1Ba_2Cu_3O_{7-y}$," Physical Review B, 40(13):9389-9392.

Hrovat, M., S. Bernik, M. Rozman and D. Kolar, 1992, "Thick Film Superconductors Based on the PbO-Modified Bi-Sr-Ca-Cu-O System with T_c(R=0) Above 77 K," Superconductive Science Technology, 5:313-317.

Hunt, V. D., 1989, *Superconductivity Sourcebook*, John Wiley & Sons, Inc., Canada, pp. 1-21.

Huse, D. A., M. P.A. Fisher, and D. S. Fisher, 1992, "Are Superconductors Really Superconducting?", Nature, 358(6387):553-559.

Iafrate, G. J., 1988, "High Temperature Superconductivity: Novel Concepts and Fundamental Issues," SPIE: Sensing, Descrimination, & Signal Processing &

Superconducting Materials & Instrumentation, 879:177-182.

Koinuma, H., T. Hashimoto, T. Nakamura, K. Kishio, K. Kitazawa, and K. Fueki, 1987, "High T_c Superconductivity in Screen Printed Yb-Ba-Cu-O Films," Japanese Journal of Applied Physics, 26(5):L761-L762.

Krishen, K. and A. Ignatiev, 1988, *World Congress on Superconductivity: Progress in High Temperature Superconductivity*, World Scientific, New Jersey, 8:141-154.

Kumakura, H., H. Shimizu, K. Takahashi, K. Togano, and H. Maeda, 1988, "Upper Critical Field of New Oxide Superconductor Bi-Sr-Ca-Cu-O," Japanese Journal of Applied Physics, 27(4):L668-669.

Lee, J. H., 1990, "Thermal Performance of a Five Year Helium Superfluid Helium Dewar for SIRTF," Cryogenics, 30:166-172.

Lynton, E. A., 1962, *Superconductivity*, London: Methuen & Co. Ltd.

Maeda, H., Y. Tanaka, M. Fukutomi, and T. Asano, 1988, "A New High-T_c Oxide Superconductor Without a Rare Earth Element," Japanese Journal of Applied Physics, 27(2):L209-L210.

Marshall, C. D., I. M. Fishman, and M. D. Fayer, 1991, "Ultrasonic Wave Propagation and Barrier-Limited Heat Flow in Thin Films of $YBa_2Cu_3O_{7-x}$," Physical Review B, 43(4):2696-2699.

Minco Products Inc., 1993, Minneapolis, MN, (512) 571-3121.

Mogro-Campero, A. and L. G. Turner, 1988, "Thin Films of Y-Ba-Cu-O on Silicon and Silicon Dioxide," Applied Physics Letter, 52(14):1185-1186.

Nagamiya, K., 1969, *Solid State Physics*, McGraw-Hill.

Patankar, S. V., 1991, *Computation of Conduction and Duct Flow Heat Transfer*, Maple Grove, MN: Innovative Research, Inc.

PATRAN, 1990, PDA Engineering, Scranton, PA.

Peacor, S. D. and C. Uher, 1989, "Thermal Conductivity of Bi-Sr-Ca-Cu-O Superconductors: Correlations with the Low-Temperature Specific-Heat Behavior," Physical Review B, 39(16):11559-11562.

Shaw-Klein, L. J., S. J. Burns, A. M. Kadin, S. D. Jacobs and D. S. Mallory, 1992,

"Anisotropic Thermal Conductivity of $YBa_2Cu_3O_{7-\delta}$ Thin Films", Superconductive Science Technology, 5:368-372.

Sherman, A., 1983, "National Aeronautics and Space Administration Needs and Trends in Cryogenic Cooling," Cryogenics, 23:348-352.

SINDA '85/FLUINT, 1985, NASA Contract NAS9-1744B, Costa Mesa, CA.

Sullivan, D. B. and J. W. Vorreiter, 1979, "Space Applications of Superconductivity," Cryogenics, 19:627-631.

Tabuchi, J. and K. Utsumi, 1988, "Preparation of Superconducting Y-Ba-Cu-O Thick Films with Preferred C-axis Orientation by a Screen-Printing Method," Applied Physics Letters, 53(7):606-608.

Uher, C., 1990, "Thermal Conductivity of High-T_c Superconductors," Journal of Superconductivity, 3(4):337-389.

Van Miltenberg, J.C., A. Schuijff, K. Kadowaki, M. Van Sprang, J.Q.A. Koster, Y.K. Huang, A.A. Menovsky, and H. Barten, 1987, "Specific Heat Measurements of High-T_c Superconductor $YBa_2Cu_3O_7$ Between 78 K and 260 K," Physica, 146B:319-323.

Volz, S. M., M. J. DiPirro, S. H. Castles, M. S. Rhee, M. G. Rysehkewitsch, and R. Hopkins, 1990, "Cryogenic On-orbit Performance of the NASA Cosmic Background Explorer (COBE)," SPIE: Cryogenic Optical Systems and Instruments IV, 1340:268-279.

Wise, S. A., I. Nolt, M. W. Hooker, G. H. Haertling, R. Selim, R. Caton and A. M. Buoncristiani, 1992, "High-Tc Thermal Bridges for Space-Borne Cryogenic Infrared Detectors," FED-Sensor Technology Branch, NASA-Langley Research Center, Hampton, Virginia.

Wu, M. K., J. R. Ashburn, C. J. Torng, P. H. Hor, R. L. Meng, L. Gao, Z. J. Huang, Y. Q. Wang, and C. W. Chu, 1987, "Superconductivity at 93 K in a New Mixed-Phase Y-Ba-Cu-O Compound System at Ambient Pressure," Physical Review Letters, 58(9):908-910.

APPENDIX A

APPENDIX A

QFLUX.FOR Program

This section includes the program QFLUX.FOR in Table A.1 which was used to determine the heat flux at the warm end of the thermal bridges for different types of materials which include the high-temperature superconductors, manganin, copper, and the substrates.

Table A.1 Program Listing for 'QFLUX.FOR'

```
**************************************************************
*
*                    HEAT FLUX DISTRIBUTION
*
*                       by Kasey M. Lee
*                       February 17, 1994
*
*  DESCRIPTION:  DETERMINE THE HEAT FLUX AT THE WARM END OF
*                THE THERMAL ISOLATOR TO MAINTAIN A TEMPERATURE
*                OF 80 K
*
**************************************************************
*
*  SET PARAMETERS
*
      DIMENSION T(100), XK(100)
*
*  SET CONSTANTS
*
      XL = 0.1524
      TOTA = 0.0
*
*     OPEN DATA FILE TO READ IN TEMPERATURE AND THERMAL
CONDUCTIVITY
```

```
*
      OPEN (1,FILE='MANGANIN.DAT')
*
*  READ IN FRIST LINE OF THE DATA FILE
*
      READ(1,*) ND
*
*  READ IN TEMPERATURE AND THERMAL CONDUCTIVITY
*
      DO 1 I=1,ND
        READ(1,*) T(I), XK(I)
 1    CONTINUE
*
*  CALCULATE HEAT FLUX
*
      NUM = ND - 1
      DO 2 I=1,NUM
        J=I+1
        IF (XK(I).LT.XK(J)) THEN
          TCMAX = XK(J)
          TCMIN = XK(I)
        ELSE
          TCMAX = XK(I)
          TCMIN = XK(J)
        END IF
        DT = ABS(T(I) - T(J))
        AREA = TCMIN * DT + (DT/2.0) * (TCMAX - TCMIN)
        TOTA = TOTA + AREA
 2    CONTINUE
*
*  PRINT OUT THE HEAT FLUX
*
      QHOT = TOTA/XL
      WRITE(*,*) 'HEAT FLUX = ', QHOT
*
*  CLOSE THE DATA FILE
*
      CLOSE(UNIT=1)
      END
```

APPENDIX B

APPENDIX B

Equations of Thermal Conductivities

This section states the equations for the thermal conductivities of the materials used in the experimental design which includes the high-temperature superconductors, the substrates, copper, and manganin. The general thermal conductivity equation is:

$$K(T)=a+bT+cT^2+dT^3+eT^4+fT^5+gT^6 \tag{6}$$

The constants a, b, c, d, e, f, and g are provided in Table B.1 on the following page for the materials used studied in this project. Since the data points are sparse for copper, only six coefficients were required to determine the thermal conductivity of this material.

The thermal conductivities were determined by using a graphics software AXUM (1993) which curve-fitted the data of the thermal conductivities provided in Figures 4.3 through 4.10 in Section 4.0 of this report.

Table B.1. Equations for the Thermal Conductivities

Materials	Coefficients for the Thermal Conductivity Equations (W/m-K)						
	a	b	c	d	e	f	g
$YBa_2Cu_3O_{7-x}$	0.1567	0.01403	0.007463	-2.510×10^{-4}	3.437×10^{-6}	-2.201×10^{-8}	5.450×10^{-11}
$BiSrCaCu_2O_x$	0.1430	0.05445	-0.003517	1.243×10^{-4}	-2.100×10^{-6}	1.665×10^{-8}	-5.035×10^{-11}
Yttrium-Stabilized Zirconia	0.4464	-0.002426	9.229×10^{-4}	-2.793×10^{-5}	3.772×10^{-7}	-2.395×10^{-9}	5.839×10^{-12}
Fused Silica	0.01565	0.002761	1.561×10^{-4}	-3.076×10^{-6}	3.403×10^{-8}	-2.009×10^{-10}	4.826×10^{-13}
Zirconia (ZrO_2)	-0.2045	0.1159	-0.001041	-2.761×10^{-5}	6.671×10^{-7}	-5.127×10^{-9}	1.367×10^{-11}
Green (Y_2BaCuO_5)	0.3558	0.07173	0.01066	-3.706×10^{-4}	4.814×10^{-6}	-2.839×10^{-8}	6.370×10^{-11}
Manganin	0.01449	0.1005	0.005584	-1.911×10^{-4}	3.283×10^{-6}	-2.880×10^{-8}	9.859×10^{-11}
Copper	297.1	-55.42	12.92	-0.5325	0.007592	-3.502×10^{-5}	0.0

APPENDIX C

APPENDIX C

Procedural Steps for Creating a Mathematical Model

This section includes the steps required to create a geometrical model in PATRAN and then be able to translate the information to be used in SINDA, the finite difference software to obtain the temperature distributions and the heat in and out of the thermal bridges.

D.1 Modeling in PATRAN

PATRAN is a software set-up for pre- and post-processing for other finite element and difference programs, such as SINDA. PATRAN was mainly used as a tool to construct the geometry of the thermal bridges and mesh the models into finite number of elements with nodes. There are three basic shapes, a line, a patch, and a hyperpatch, which are used to construct any type of geometry. A patch is a two-dimensional surface which can be rectangular or circular. A hyperpatch is a three-dimensional solid. There are various commands, such as tracing and extruding, that can be used to construct these three basic geometries. This section provides an example of the simplest form of creating these basic shapes. For the other methods and help, refer to the PATRAN manuals.

Starting in PATRAN

After having logged into the workstation, follow the subsequent steps to run the

software PATRAN. Remember to go to the X-Windows to take the full advantage of using PATRAN. PATRAN will not run within any other displays.

1. Type "PATRAN" in the command line in the workstation. The screen will ask for the mnemonic device.

2. Enter "xwn".

3. The PATRAN software display is activated on the monitor. Type "GO". Then type "1" for a new file or "2" for an old file. Since this is the first run of using PATRAN, type "1".

Creating a Geometrical Model

4. Select "1" for Geometry. Then the screen will display "Input Command or End". If you wish to end this exercise at any time, select the end options or type "END". For now, the following will include the steps to create a line, a patch, or a hyperpatch.

5. The general command for creating a line, a patch or a hyperpatch is:

Shape, ID, , dx/dy/dz/ox/oy/oz

where: Shape = LINE, PATCH, or HPAT
ID = an identification number for the shape (this number is arbitrary)
dx/dy/dz = the length of the shape in the x, y, or z direction, respectively
ox/oy/oz = the originating coordinate of the shape (this is the point where the dx/dy/dz values are added in order to create the shape)

6. Use the commands provided in step 5 to create the entire model or type "END" to return to the main menu.

Creating the Meshed Elements and Nodes

7. The general command for creating elements and nodes are:

MESH, L-ID/P-ID/HP-ID, ELEM, ISO, Length, Prop-ID or MAT-ID

where: L-ID = a line with an identification number (e.g. L10 which indicates the line with ID of 10)
P-ID = a patch with an identification number
HP-ID = a hyperpatch with an identification number
ELEM = the shape of the elements (choices are quad for surfaces and hex for solids)
ISO = the type of mesh (isoparametric is chosen because it is the best congruent form of meshing)
Length = the length of the element
Prop-ID or
MAT-ID = for boundary surfaces, it is better to place a property identification number which can be any arbitrary number

for solids (hyperpatches), place a material-ID, by typing "M" followed by the material identification number (e.g. M1 indicates that the elements meshed in this commands will all have the material ID of 1)

8. Type "EQUIV". Select "2" for Geometric equivalencing and then, "1" for all. Answer "Y" to any question that the program prompts you during this process. This process is done to insure that there are no duplicate nodes and so that a minimum number of nodes are created for the model.

9. This step is included for boundary conditions. If there are no boundary conditions in the problem, proceed on to the next step. Two consecutive steps are required to create the boundary conditions. First general command is:

PFEG, P-ID, ELEM, MAT-ID//thk, Prop-ID

where P-ID = a patch identification number (e.g. P1)
ELEM = the shape of the elements created for the patch (QUAD or HEX)
MAT-ID = a material identification number (this option is left blank if the boundary condition is a fixed temperature)
thk = a thickness of the patch
Prop-ID = a property identification number which is the same number assigned when the patches were meshed

The second general command depends on the type of boundary conditions. Since a fixed temperature and a heat flux are the most common ones, they will be provided as examples of creating the boundary conditions.

For a fixed temperature, type the following:

DFEG, P-ID, TEMP/E, temp/-1

by entering the patch identification number for P-ID (e.g. P10) and the value for the temp. The "-1" at the end of the command indicates that this is a boundary condition.

For a heat flux, type the following command:

DFEG, P-ID, HEAT/E, heat/1/2

by entering the patch identification number for P-ID and the value of the heat flux for "heat". The "1/2" option at the end of the command indicates that it is a heat source on the boundary and that it is in the form of Watts per area (W/A).

10. The general command for creating the material properties is as follows:

PMAT, MAT-ID, ANI, 3, C, 1.0,,,3, k,1.0

where MAT-ID = the material identification number
C = the SINDA array number for the specific heat of the element material
k = the SINDA array number for the thermal conductivity of the element material

The SINDA array number is a number in the program SINDA which provides the data for the material properties required to do the analysis. For instance, the specific heat for a certain type of material in SINDA can be represented by "10". This array number will give the values of the specifics heats at various temperatures for this specific material.

11. Select the end options or type "end" to return to the main menu.

Translating PATRAN Data to SINDA

12. The following steps provide a way to translate the information created in PATRAN into SINDA to be able to run the finite difference model. The first step is to create a neutral file by selecting "5" for SINDA option.

13. Select "1" for neutral file and then, "1" again for output. Select "1" for all and answer "y" to the questions prompted in this procedure.

14. After the neutral file has been created, the program will prompt for a translation option, to or from SINDA. Make certain that a skeleton file with the same basename of the SINDA file that you are creating exists. For instance, if a SINDA input file "example.sin" is going to be created, then a skeleton file by the name "example.ssk" must exist before the translator is activated. For now, select "2" to translate from PATRAN to SINDA. A new window for the translator, PATSIN, from PATRAN to SINDA program is displayed on the screen. Hit the enter key once. Select "1" for the translation option. Enter the basename of the filename for the SINDA input file (e.g. example for example.sin). Then the screen will ask if the neutral file is the same as the SINDA input file, type in the appropriate neutral filename if it is different. The translator will process the information from the neutral file to the SINDA input file. When it has completed this task, error messages will be displayed. The error messages are usually saved under "patsin.msg". Then select "3" to end the translation and return to PATRAN.

15. Select "6" to stop running PATRAN. If there were errors obtained in creating the SINDA input file, make certain these are corrected before proceeding on to the next phase of the modeling which is running SINDA.

Running SINDA

16. First edit the SINDA input files to follow the similar formats of the SINDA input file provided as Appendix C in this report. Send the input file to NASA-LaRC to run SINDA.

17. Inside the NASA-LaRC account, type the following:

    /bin/time /usr/Sinda/bin/sinda basename.sin >& basename.opp &

    The basename is the name of the SINDA input file. This step allows the program to be run in the background. The basename.opp is the file where the information processed in the run is saved. This file allows a user to determine where the errors occurred if any did occur during the run.

    In order to run several programs, it is better to run them consecutively and not all at once because it slows the process. The command to use is the "sleep" command which can be implemented using the following command:

    (sleep 3600; /bin/time /usr/Sinda/bin/sinda basename.sin >& basename.opp &)

    The only difference between this command and the one mentioned prior in this step is the parenthesis and the "sleep 3600". This particular sleep command states

that this input file will not be processed through SINDA until 3600 seconds have passed. The time allocated for the process to occur is arbitrary, i.e. the user can type in any time and not just 3600 seconds.

18. The results from the SINDA is the basename.sot file which is the output file that contains the temperature distributions and the energy balance of the model.

SINDA to PATRAN Translation

19. First transfer the SINDA output file from NASA-LaRC to VPI & SU.

20. The translator from SINDA output file to PATRAN is SINPAT. Therefore, type "sinpat" on the workstation.

21. Select "1" to translate the results. Type in the basename of the file (e.g. example is the basename of the output file "example.sot"). Enter "y" and then hit the enter key twice for the next two prompts. Type "2" for the case to be translated. The elements and nodes files, example2.els.1 and example2.nod.1 respectively, are created. Type "q" to exit to the main menu of SINPAT. If the user wishes to translate more output files, then repeat the steps outlined in this procedural step. If not, then select "7" to end the program.

    Note that there may be more than 2 time indices for the output file. If so, it means that the criteria set for the model were not met during the analysis. This means that the results obtained are not accurate because the nodal temperatures have not converged and/or the energy balances have not been satisfied. It is recommended then that the user tighten the criteria in the SINDA input file and restart the process from step 16 until the temperatures have converged and the energy balance has been fulfilled.

Display Temperature Distributions (Results) in PATRAN

22. Repeat steps 1 through 3 except in step 3, select "2" to recall the geometry file which has already been created.

23. Type "SET,XFR,ON". This option allows the temperature distributions to be displayed in continuous tones of colors. In order to view the temperatures better, type "SET,LABELS,OFF", "SET,LINES,OFF", "NODES,1T#,ERASE", and "SET,AHIDE,OFF".

24. Select "4" from the main menu to display the results. Type "2" for external data,

"4" for nodal, "1" for the first column, and "1" for contours. Type the nodal filename that you wish to display, for example, type "example2.nod.1". Then type "1" for auto and "7" for plot. The temperature distributions along the model are displayed.

25. The hardcopy for the temperature distributions can be obtained by typing "SET,HARDCOPY,ON". Re-select "7". Select the end options and/or type "end" to exit from PATRAN.

26. The hardcopy from PATRAN is saved as patran.hrd.# where # stands for the number related to the file created. Type "postscript" to translate the patran.hrd file to postscript file. Inside the postscript software, type "invc" to obtain a color postscript file of the results. The resulting postscript file is ps.plt.# where # relates to the number of the file that has been run.

APPENDIX D

APPENDIX D

Sinda Input File

This section contains the SINDA input file used to determine the temperature distributions of the thermal bridges and the heat transfer in and out of the thermal bridges.

Table D.1. Sinda Input File

```
HEADER OPTIONS DATA
TITLE Thermal Isolator Temperature and Heat Flux Distribution
C
      MODEL = thiso
      OUTPUT = model1.sot
C
HEADER CONTROL DATA,GLOBAL
C
      TIMEO = 0.0*3600.
      TIMEND = 0.0*3600.
      UID = SI
      NLOOPS = 10000
      ABSZRO = -273.15
C
C  CRITERIA FOR CONVERGENCE
C
      ARLXCA = 0.002
      DRLXCA = 0.002
      EBALSA = .01
      EBALNA = .01
C
C**********************************************************************
******
C
HEATER ARRAY DATA,INST
C
C  BEGIN NON PATSIN GENERATED ARRAY DATA
```

```
C ************** METRIC ***************
C
C THERMAL CONDUCTIVITIES IN W / cm K
C
C REFERENCES:   1 - Christopher Newport University
C               2 - Emerson & Cunnings Catalogue
C               3 - Caton and Selim Report
C               4 - Minco Products
C
C
C THERMAL CONDUCTIVITY OF kapton insulation (ref. 4)
      21 = 25.0, 0.16
C
C THERMAL CONDUCTIVITY OF YBaCuO (ref. 1)
      21 = -269.15, .315, -252.83, 1.94, -251.74, 2.06,
           -250.52, 2.17,
           -249.3, 2.3, -248.11, 2.39, -246.9, 2.47,
           -245.69, 2.6, -244.54, 2.69, -243.33, 2.76,
           -242.11, 2.91, -240.82, 2.97, -239.6, 3.05,
           -238.41, 3.13, -237.08, 3.18, -235.88, 3.24,
           -234.55, 3.3, -233.33, 3.35, -232.02, 3.39,
           -230.83, 3.46, -229.49, 3.48, -228.31, 3.51,
           -227.01, 3.55, -225.81, 3.57, -224.49, 3.61,
           -223.27, 3.61, -221.99, 3.6, -220.79, 3.61,
           -219.48, 3.63, -218.27,3.63, -216.95, 3.63,
           -215.75, 3.62, -214.46, 3.62, -213.24, 3.62,
           -211.93, 3.61, -210.74, 3.62, -209.43, 3.6,
           -208.23, 3.6, -206.92, 3.58, -205.72, 3.58,
           -204.51, 3.57, -203.21, 3.55, -202.02, 3.54,
           -200.8, 3.54, -199.5, 3.53, -198.28, 3.51,
           -197.0, 3.52, -195.79, 3.51, -194.49, 3.5,
           -193.3, 3.49, -191.99, 3.47, -190.78, 3.46,
           -189.47, 3.45, -188.28, 3.46, -186.97, 3.43,
           -185.76, 3.42, -184.49, 3.42, -183.27, 3.41,
           -181.96, 3.39, -180.75, 3.37, -179.47, 3.37,
           -178.25, 3.34, -176.93, 3.33, -175.73, 3.33,
           -174.43, 3.32, -173.21, 3.29, -171.95, 3.29,
           -170.71, 3.29, -169.51, 3.28, -168.21, 3.26,
           -167.02, 3.25
C
C THERMAL CONDUCTIVITY OF BiSrCaCu(2)O(x) (ref.  )
      21 = -269.15, .312, -250.15, 0.56, -225.65, 0.88,
           -212.15, 1.00,
```

```
     -205.15, 1.02, -195.15, 1.02, -173.15, 0.97
C
C  THERMAL CONDUCTIVITY OF Yttrium Stabilized Zirconia (YSZ1) (ref.1)
      11 = -269.15, .444, -263.15, .5, -255.58, .59,
     -254.55, .58, -252.82, .59,
     -251.22, .61, -249.41, .64, -247.61, .64,
     -246.01, .67, -244.26, .68, -242.51, .71,
     -240.69, .73, -238.97, .74, -237.11, .76,
     -235.37, .77, -233.59, .79, -231.87, .8,
     -230.06, .8, -228.35, .81, -226.53, .83,
     -224.79, .84, -222.99, .84, -221.29, .85,
     -219.5, .86, -217.8, .87, -215.96, .88,
     -214.24, .88, -212.43, .89, -210.72, .9,
     -208.9, .91, -207.22, .91, -205.42, .93,
     -203.71, .94, -202.0, .94, -200.32, .96,
     -198.48, .96, -196.81, .98, -194.99, .99,
     -193.29, .99, -191.5, 1.01, -189.78, 1.02,
     -187.97, 1.04, -186.26, 1.04, -184.48, 1.05,
     -182.75, 1.06, -180.95, 1.08, -179.25, 1.09,
     -177.45, 1.1, -175.71, 1.11, -173.93, 1.11,
     -172.23, 1.13, -170.39, 1.14, -168.7, 1.15,
     -167.01, 1.17, -165.19, 1.18, -163.48, 1.18,
     -161.71, 1.2, -159.95, 1.21, -158.19, 1.22,
     -156.46, 1.25, -154.67, 1.26, -152.98, 1.27,
     -151.15, 1.28
C
C  THERMAL CONDUCTIVITY OF Fused Silica (ref.1)
      11 = -269.15, .0275, -255.89, .1, -254.54, .11,
     -252.75, .12,
     -251.05, .12, -249.35, .14, -247.59, .15,
     -246.0, .16, -244.23, .17, -242.5, .18,
     -240.68, .19, -238.98, .2, -237.22, .22,
     -235.41, .23, -233.66, .24, -231.87, .26,
     -230.16, .27, -228.33, .28, -226.65, .3,
     -224.8, .31, -223.12, .32, -221.3, .33,
     -219.62, .34, -217.8, .36, -216.08, .37,
     -214.27, .38, -212.58, .39, -210.73, .4,
     -209.03, .41, -207.24, .43, -205.52, .44,
     -203.84, .44, -202.07, .46, -200.34, .47,
     -198.63, .48, -196.83, .49, -195.13, .51,
     -193.33, .52, -191.63, .54, -189.79, .55,
     -188.08, .56, -186.29, .57, -184.57, .58,
     -182.77, .59, -181.07, .61, -179.27, .61,
```

```
     -177.54, .62, -175.75, .64, -174.03, .65,
     -172.25, .66, -170.51, .67, -168.82, .68,
     -167.05, .69, -165.32, .7, -163.51, .71,
     -161.82, .72, -160.01, .74, -158.28, .75,
     -156.49, .75, -154.78, .77, -152.99, .78,
     -151.28, .79
C
C  THERMAL CONDUCTIVITY OF Green (211) Phase (ref. 1)
      11 = -269.15, .787, -256.65, 3.12, -250.65, 4.24,
           -245.65, 4.93,
           -240.65, 5.68, -235.15, 6.13, -223.15, 6.5,
           -218.15, 6.38, -209.15, 6.13, -199.15, 5.68,
           -185.15, 5.13, -169.15, 4.68, -160.65, 4.38,
           -153.15, 4.2
C
C  THERMAL CONDUCTIVITY OF Manganin Wires (ref. 3)
      11 = -269.15, .5, -263.15, 1.4, -253.15, 3.2,
           -243.15, 4.9, -233.15, 6.6, -223.15, 8.2,
           -213.15, 9.6, -203.15, 10.9, -193.15, 11.9
C
C  THERMAL CONDUCTIVITY OF Stycast 2850 epoxy 24LV (ref. 2)
      41 = -233.15, 1.00416
C
C  THERMAL CONDUCTIVITY OF OFHC Copper (ref. 4)
      31 = -269.15, 250., -263.15, 575., -253.15, 1200.,
           -245.15, 1250.0, -203.15, 500.0,
           -173.15, 425.0
C
C  THERMAL CONDUCTIVITY OF ZIRCONIA (YSZ2) (ref. 1)
      51 = -269.15, .24, -257.06, 1.3, -254.55, 1.52,
          -252.56, 1.61,
           -250.84, 1.7, -249.08, 1.76, -247.37, 1.82,
           -245.6, 1.91, -243.97, 2.0, -242.17, 2.07,
           -240.33, 2.1, -238.63, 2.13, -236.89, 2.19,
           -235.14, 2.2, -233.37, 2.24, -231.67, 2.26,
           -229.82, 2.27, -228.13, 2.29, -226.3, 2.31,
           -224.55, 2.31, -222.75, 2.32, -221.06, 2.32,
           -219.26, 2.33, -217.56, 2.34, -215.76, 2.34,
           -214.04, 2.31, -212.26, 2.33, -210.54, 2.33,
           -208.73, 2.33, -207.03, 2.34, -205.23, 2.34,
           -203.53, 2.33, -201.85, 2.34, -200.16, 2.37,
           -198.31, 2.36, -196.64, 2.36, -194.85, 2.37,
           -193.14, 2.37, -191.33, 2.38, -189.62, 2.4,
```

```
            -187.83, 2.41, -186.12, 2.43, -184.32, 2.42,
            -182.6, 2.42, -180.81, 2.43, -179.12, 2.45,
            -177.3, 2.46, -175.57, 2.46, -173.78, 2.46,
            -172.08, 2.47, -170.28, 2.49, -168.57, 2.49,
            -166.87, 2.5, -165.07, 2.5, -163.36, 2.51,
            -161.57, 2.53, -159.83, 2.52, -158.05, 2.55,
            -156.32, 2.56, -154.55, 2.56, -152.85, 2.59,
            -151.02, 2.58
C
C  Specific Heat Data
C
C  Superconductor or kapton insulation Specific Heat
       20 = 25.0, 1.00
C
C  Substrate or manganin Specific Heat
       10 = 25.0, 1.00
C
C  Copper Specific Heat
       30 = 25.0, 1.00
C
C  Stycast Specific Heat
       40 = 25.0, 1.00
C
C  Zirconia Specific Heat
C       50 = 25.0, 1.00
C
C  BRING IN NODE, CONDUCTOR, AND SOURCE DATA
C
include mang.dat
C
C*****************************************************************
HEADER OPERATIONS DATA
BUILD THISO, INST
C
C  EXECUTE SOLUTION SUBROUTINES
C
C  SET INITIAL TEMPERATURES FOR ALL NODES
F      DO 100 I = 1, NNOD
F      T(I) = -269.15
F100   CONTINUE
C
C
       CALL STDSTL
```

```
C
C*****************************************************************
HEADER OUTPUT CALLS, INST
C
C  CHANGE TEMPERATURE TO KELVIN
F      DO 200 ITEST = 1, NNOD
F      T(ITEST) = T(ITEST) + 273.15
F200   CONTINUE
C
C  PRINT TEMP TO OUTPUT FILE
       IF (TIMEN.EQ.TIMEND) CALL TPRINT ('INST')
C
C  CHANGE TEMPERATURE BACK TO CELSIUS
F      DO 300 ITEST = 1, NNOD
F      T(ITEST) = T(ITEST) - 273.15
F300   CONTINUE
C
C  END
C
```